Control Synthesis for Hypersonic Vehicle Flight Testing with Input–Output-Sampled Nonlinearities

Sze Kwan Cheah,* Diganta Bhattacharjee,† Maziar S. Hemati,‡ and Ryan J. Caverly§
University of Minnesota, Minneapolis, Minnesota 55455

https://doi.org/10.2514/1.G008331

The flight testing of hypersonic vehicles is challenging due to the nonlinear, uncertain, and possibly unstable dynamics of these vehicles. This paper presents a control synthesis method for a hypersonic vehicle with the purpose of guaranteeing robust stability during flight testing when accurate analytic vehicle models are unavailable. Conventional model-based approaches typically rely on curve fitting of numerical simulation and test data, which can introduce inaccuracies. Our proposed approach assumes knowledge of the linear form of the ordinary differential equation and uses quadratic constraints to bound sampled data that accounts for the nonlinear and uncertain portion of the model for controller synthesis by iteratively solving convex semidefinite programs. A numerical example demonstrating the effectiveness of the proposed method is performed before applying the technique to a nonlinear hypersonic vehicle found in the literature. Using the synthesized stabilizing controller, we demonstrate that the vehicle states remain within a certified bound given a known harmonic excitation when initiated from a quantified set of allowable initial conditions. Based on these simulation results, our proposed control synthesis method shows promise in ensuring robustness when performing hypersonic vehicle flight testing.

I. Introduction

HYPERSONIC vehicles traveling at speeds greater than Mach 5 are currently under development for commercial and defense applications. Developing robust feedback controllers for these experimental vehicles is challenging due to their highly uncertain, nonlinear, and coupled dynamics, which stems from the difficulty in capturing complex aerothermodynamics at hypersonic speeds. This is especially true for prototype hypersonic flight vehicles, where opportunities to collect flight test data to refine the vehicle model are limited and the available flight tests are limited in duration. In this scenario, it is essential to develop flight maneuvers (i.e., excitation inputs) that sufficiently excite the vehicle's dynamics while also designing a feedback controller that ensures closed-loop stability and safety-critical constraints on the vehicle response are maintained (i.e., the vehicle is kept within a safe flight envelope) in the presence of relatively large model uncertainty and nonlinearities.

The success of model-based control methods depends heavily on the fidelity of the underlying model. Work was performed notably by the authors of Refs. [2,3] to model a hypersonic vehicle with flexible dynamics and the sensitivity to varying mass. This was followed by other modeling papers such as [4] that used piston theory to calculate pressure on the vehicle surface. An early nonlinear model of the longitudinal dynamics of a hypersonic vehicle was developed by the authors of Ref. [5]. Model-based control methods are found in the literature for hypersonic vehicles, notably [6], which features a robust control design. A backstepping controller with fault tolerance was studied in [7]. Adaptive sliding model control [8,9] and linearization-based techniques [10,11] have also been considered. While these controllers address the control challenges associated with the nonlinear dynamics of a hypersonic vehicle, they rely on knowledge of an analytic form of the system's nonlinearities, while accounting for uncertainty in certain model parameters. This is a potential limitation when working with dynamic models generated from computational fluid dynamics (CFD) simulations [12] or experimental wind tunnel data [13], which typically provide modeling information at specific points within a parametric space (e.g., a lookup table of aerodynamic coefficients), rather than an analytic model. Curve fitting the data provides a coarse approximation of the best available data as deviations from the fit are ignored. In the case of a hypersonic flight test, it may be required to design flight test controllers based on simulation and test data, which limits the use of traditional nonlinear control approaches.

Data-driven techniques are now becoming increasingly popular for control systems [14–17]. For example, strategies are being developed to determine the input–output properties of dynamic systems from sampled data, including identifying dissipation inequalities [18] and passivity metrics [19]. Other more recent work utilizes a neural control scheme [20] or fuzzy logic system [21]. Once the input–output properties of a system or a portion of the system are identified from data, stability theorems (e.g., passivity theorem, circle criterion) can be leveraged to design controllers that ensure closed-loop stability or performance properties. This input–output approach allows for a "black box" interpretation of the complicated, nonlinear, and possibly uncertain aspects of the system while allowing for a framework in which stabilizing controllers can be designed.

This paper makes use of input–output sampling to develop a control design method for the stabilization of a hypersonic flight test vehicle with nonlinear dynamics. The motivation here is a flight test where input–output data are to be collected for nonlinear system identification, which necessitates a flight test vehicle response that is not well-captured by a linear model. This results in the need for nonlinear analysis tools to be able to certify the safety of the flight test. In this work, we aim to design a linear feedback controller that provides a certification of transient boundedness in the states of the nonlinear system during such as a flight test. Our proposed approach follows a method similar to what is described in [22], where the nonlinear dynamics of the hypersonic vehicle are modeled as perturbations to a known linear time-invariant (LTI) linearization of the system within a linear fractional transformation (LFT) framework. Integral quadratic constraints [23] provide a framework to quantify the input–output properties of an operator (e.g., a nonlinear function or a dynamic system). A subset of this framework is the characterization of static and memoryless nonlinearities using quadratic constraints (QCs) [23] that are satisfied pointwise at every instance in

Presented as Paper 2014-1589 at the AIAA SciTech 2024 Forum, Orlando, FL, January 8–12, 2024; received 6 March 2024; accepted for publication 10 October 2024; published online 16 January 2025.

*Ph.D. Student, Department of Aerospace Engineering and Mechanics; cheah013@umn.edu. Student Member AIAA.

†Postdoctoral Research Associate, Department of Aerospace Engineering and Mechanics; dbhattac@umn.edu. Member AIAA.

‡Associate Professor, Department of Aerospace Engineering and Mechanics; mhemati@umn.edu. Associate Fellow AIAA.

§Assistant Professor, Department of Aerospace Engineering and Mechanics; rcaverly@umn.edu. Member AIAA (Corresponding Author).

time. In this work, the vehicle's nonlinear dynamics are partitioned into a linear dynamic model and another portion that contains all nonlinearities. Input–output samples of the nonlinearities are used to quantify norm-bound QCs that characterize the nonlinearities within a local region about an equilibrium trim condition. Control synthesis is a challenge due to the fact that the perturbations are described with input–output data, and the sampling range of these data is dependent on the choice of controller. This poses a problem, as the sample-based input–output characterization of the perturbations requires a controller to be chosen *a priori*, while a controller cannot be synthesized until this input–output characterization is known. The causality dilemma is resolved by first prescribing a closed set for the states and inputs for use in sampling and subsequent characterization of QC properties of the nonlinearities. By constraining the maximum singular value of the controller during synthesis, this ensures that the control input always remains within the prescribed range of sampled inputs. As the synthesis problem is nonconvex, it is resolved by iteratively solving three semidefinite programs (SDPs) that are obtained through convex relaxations.

Harmonic excitation is often used for flight testing of prototype aircraft for system identification and stability margin determination [24]. These flight test maneuvers are executed by applying carefully designed input time series to the aircraft's control inputs. Oftentimes, these inputs are the sum of harmonic signals with unique frequencies and phase shifts designed to be mutually orthogonal both in the time and frequency domain. These harmonic excitations on the aircraft control inputs are sometimes made in addition to the system's feedback control input, as the aircraft can be open-loop unstable. A feedback controller that provides a guarantee of state boundedness is useful to avoid instability and catastrophic failures induced by perturbing the vehicle outside of the flight envelope the feedback controller is designed for. Complicating this problem further is the presence of nonlinearities in the system's dynamics, which are often difficult to model and test for. Moreover, these nonlinearities cannot be ignored if the purpose of the flight test is to obtain input–output data further from the equilibrium point in order to refine the nonlinear model through a system identification process. It is worth noting that in [25], the "truth model" of the hypersonic vehicle was developed by the authors of Ref. [5] using physics-based first principles. Even so, there were significant differences in the drag and lift plots when comparing the truth model to the "full fit" and "simplified fit" models. The truth model is not publicly available, but the control-oriented model and associated coefficients are published in [25], allowing us to demonstrate how sampling the control-oriented model, not just analytic curve-fitted data, can be incorporated into the control synthesis procedure.

The main contributions of this work in comparison to the control methodology presented in [22] include 1) the manner in which weightings and uncertainty decomposition are employed to make the hypersonic vehicle model in [25] amenable to the control synthesis method in [22] and 2) the development of an analysis and synthesis framework that extends the work in [22] to account for the exogenous excitation signals relevant to a hypersonic vehicle flight test. Our proposed control synthesis method is able to account for the sampled nonlinearities of the control-oriented hypersonic model in [25] by providing a guarantee that the vehicle states remain bounded within a specified region in the presence of harmonic excitation signals similar to [24]. The synthesized controller provides a means of performing flight test maneuvers of a nonlinear hypersonic vehicle while adhering to safety-critical constraints. In contrast to traditional nonlinear control techniques, this control synthesis method does not require an analytic representation of the vehicle's nonlinear dynamics.

The rest of this paper is organized in the following manner: Important preliminaries, including notation, and a description of the problem statement are presented in Sec. II. Section III details the system with an appended exogenous input signal treated as a general external signal, filtered external signal, and harmonic excitation signal. Section IV proposes control synthesis methods for the three types of exogenous inputs with relaxations of the linear matrix inequalities (LMIs) in Sec. V. The proposed algorithm is first applied to a two-state nonlinear model in Sec. VI to clearly demonstrate the effect of different choices in the characterization of the exogenous input signal when synthesizing the controller. Section VII provides numerical results with the proposed control synthesis method applied to the hypersonic vehicle model in [25]. Given the complexities of this model, only one of the methods for characterizing the exogenous input signal is successfully implemented. This is followed by concluding remarks in Sec. VIII.

II. Preliminaries

This section presents the notation that will be used throughout the paper along with a general model description and the problem statement.

A. Notation

The symbol $\mathcal{N}_n$ is a shorthand for the set of natural numbers $\{1, 2, \ldots, n\}$. The matrix of zeros and identity matrix are, respectively, written as $\mathbf{0}$ and $\mathbf{1}$. A column matrix of zeros with the ith entry of 1 is denoted as $\mathbf{1}_i$. Matrices and vectors are represented in bold with matrices capitalized and vectors lowercase (e.g., $\boldsymbol{A} \in \mathbb{R}^{n\times m}$ and $\boldsymbol{b} \in \mathbb{R}^n$). Symmetric n-by-n matrices are represented by $\boldsymbol{A} \in \mathbb{S}^n$, and their positive or negative definiteness is denoted by $\boldsymbol{A} > 0$ or $\boldsymbol{A} < 0$, respectively. The maximum singular value of $\boldsymbol{A}$ is denoted by $\overline{\sigma}(\boldsymbol{A})$. A given ellipsoid centered at the origin is denoted as $\mathcal{E}_n(\boldsymbol{E}) = \{\boldsymbol{x} \in \mathbb{R}^n \,|\, \|\boldsymbol{E}^{-1}\boldsymbol{x}\|_2 \leq 1\}$ and $\mathcal{B}_n(r) = \{\boldsymbol{x} \in \mathbb{R}^n \,|\, \|\boldsymbol{x}\|_2 \leq r\}$ denotes the closed unit-norm ball of radius r in $\mathbb{R}^n$. The finite time signal norm is expressed as $\|\boldsymbol{x}\|_{2T} = \int_0^T \|\boldsymbol{x}\|_2 \, \mathrm{d}t$.

B. Problem Statement

The remainder of this section focuses on outlining a mathematical description of the problem of interest in this work; particularly, we wish to design a state-feedback controller that ensures boundedness in the presence of excitation inputs and nonlinear dynamics that may only be known through input–output samples. To this end, consider a dynamic system governed by the differential equation $\dot{\boldsymbol{x}} = \boldsymbol{f}(\boldsymbol{x}, \boldsymbol{u})$. The dynamic system may be represented about the equilibrium point $(\boldsymbol{x}_0, \boldsymbol{u}_0)$ without any approximation as

$$\delta\dot{\boldsymbol{x}} = \boldsymbol{A}\delta\boldsymbol{x} + \boldsymbol{B}_1\delta\boldsymbol{u} + \boldsymbol{\Delta}(\delta\boldsymbol{x}, \delta\boldsymbol{u}) \tag{1}$$

where $\delta\boldsymbol{x} = \boldsymbol{x} - \boldsymbol{x}_0$, $\delta\boldsymbol{u} = \boldsymbol{u} - \boldsymbol{u}_0$, and $\boldsymbol{\Delta}(\delta\boldsymbol{x}, \delta\boldsymbol{u}) = \boldsymbol{f}(\boldsymbol{x}, \boldsymbol{u}) - (\boldsymbol{A}\delta\boldsymbol{x} + \boldsymbol{B}_1\delta\boldsymbol{u})$. The state matrix $\boldsymbol{A} = \partial\boldsymbol{f}/\partial\boldsymbol{x}$ evaluated at $(\boldsymbol{x}_0, \boldsymbol{u}_0)$ and control matrix $\boldsymbol{B}_1 = \partial\boldsymbol{f}/\partial\boldsymbol{u}$ evaluated at $(\boldsymbol{x}_0, \boldsymbol{u}_0)$ capture the linearized dynamics about the equilibrium, while $\boldsymbol{\Delta}(\delta\boldsymbol{x}, \delta\boldsymbol{u})$ captures all the higher-order terms. It is assumed that the pair $(\boldsymbol{A}, \boldsymbol{B}_1)$ is stabilizable. It is worth noting that $\boldsymbol{\Delta}(\delta\boldsymbol{x}, \delta\boldsymbol{u})$ approaches zero as $\delta\boldsymbol{x} \to \mathbf{0}$ and $\delta\boldsymbol{u} \to \mathbf{0}$. As the nonlinear dynamics approach dynamic equilibrium, the system's dynamics approach its linearized dynamics. It is also emphasized that the nonlinear dynamics in Eq. (1) are an exact reformulation of the system's nonlinear dynamics $\dot{\boldsymbol{x}} = \boldsymbol{f}(\boldsymbol{x}, \boldsymbol{u})$ due to the specific definition of $\boldsymbol{\Delta}(\delta\boldsymbol{x}, \delta\boldsymbol{u})$.

The nonlinearities may be distributed into n_p input–output functions $p_i = \Delta_i(\boldsymbol{v}_i)$, $i \in \mathcal{N}_{n_p}$ that can be individually characterized by sampled data of the respective input–output functions. Their contributions to the nonlinear equations of motion appear via the signal $\boldsymbol{p} = \boldsymbol{\Delta}(\boldsymbol{v}) = [\Delta_1(\boldsymbol{v}_1)\, \Delta_2(\boldsymbol{v}_2) \;\; \cdots \;\; \Delta_{n_p}(\boldsymbol{v}_{n_p})]^\mathsf{T} \in \mathbb{R}^{n_p}$, where $\boldsymbol{v} = [\boldsymbol{v}_1^\mathsf{T} \;\; \boldsymbol{v}_2^\mathsf{T} \;\; \cdots \;\; \boldsymbol{v}_{n_p}^\mathsf{T}]^\mathsf{T}$ is dependent on $\boldsymbol{x}$ and $\boldsymbol{u}$. The reformulation of Eq. (1) is

$$\delta\dot{\boldsymbol{x}} = \boldsymbol{A}\delta\boldsymbol{x} + \boldsymbol{B}_1\delta\boldsymbol{u} + \boldsymbol{B}_2\boldsymbol{p} \tag{2}$$

$$p_i = \Delta_i(\boldsymbol{v}_i), \; i \in \mathcal{N}_{n_p} \tag{3}$$

$$\boldsymbol{v}_i = \boldsymbol{E}_i(\boldsymbol{C}_i\delta\boldsymbol{x} + \boldsymbol{D}_i\delta\boldsymbol{u}), \; i \in \mathcal{N}_{n_p} \tag{4}$$

where the matrices $\boldsymbol{C}_i$ and $\boldsymbol{D}_i$ determine the inputs to the functions $\Delta_i(\boldsymbol{v}_i)$. The weighting matrix $\boldsymbol{E}_i$ is introduced to normalize the vector $\boldsymbol{v}_i$ such that the norm is not greater than 1. This provides a

more balanced weighting of each variable since the states may be composed of variables with different units. Setting $\boldsymbol{E}_i$ as a diagonal matrix with each entity being the inverse of the maximum magnitude of the corresponding state is a reasonable weighting matrix.

The higher-order terms are represented in the function Δ_i and may be determined in various manners. When analytical equations are available, the equation of motion may be decomposed into a vector sum of n_p equations:

$$\delta\dot{\boldsymbol{x}} = \boldsymbol{f}(\boldsymbol{x},\boldsymbol{u}) = \sum_{i=1}^{n_p} \boldsymbol{f}_i(\boldsymbol{x},\boldsymbol{u}),\ i \in \mathcal{N}_{n_p} \tag{5}$$

$$\boldsymbol{f}_i(\boldsymbol{x},\boldsymbol{u}) = \boldsymbol{f}_i(\boldsymbol{x}_0,\boldsymbol{u}_0) + \left.\frac{\partial \boldsymbol{f}_i}{\partial \boldsymbol{x}}\right|_{(\boldsymbol{x}_0,\boldsymbol{u}_0)} \delta\boldsymbol{x} + \left.\frac{\partial \boldsymbol{f}_i}{\partial \boldsymbol{u}}\right|_{(\boldsymbol{x}_0,\boldsymbol{u}_0)} \delta\boldsymbol{u} + \Delta_i(\boldsymbol{x},\boldsymbol{u}) \tag{6}$$

$$= \boldsymbol{f}_i(\boldsymbol{x}_0,\boldsymbol{u}_0) + \bar{\boldsymbol{A}}_i\delta\boldsymbol{x} + \bar{\boldsymbol{B}}_i\delta\boldsymbol{u} + \Delta_i(\boldsymbol{x},\boldsymbol{u}) \tag{7}$$

Rearranging this equation yields a description of the nonlinearities in the form

$$\Delta_i(\boldsymbol{x},\boldsymbol{u}) = \boldsymbol{f}_i(\boldsymbol{x},\boldsymbol{u}) - (\bar{\boldsymbol{A}}_i\delta\boldsymbol{x} + \bar{\boldsymbol{B}}_i\delta\boldsymbol{u} + \boldsymbol{f}_i(\boldsymbol{x}_0,\boldsymbol{u}_0)) \tag{8}$$

Note that $\bar{\boldsymbol{A}}_i = \partial \boldsymbol{f}_i/\partial \boldsymbol{x}$ and $\bar{\boldsymbol{B}}_i = \partial \boldsymbol{f}_i/\partial \boldsymbol{u}$. The sum of partial derivatives is related to the terms in Eq. (2) through the relationships $\sum \boldsymbol{f}_i(\boldsymbol{x}_0,\boldsymbol{u}_0) = \boldsymbol{0}$, $\sum \bar{\boldsymbol{A}}_i = \boldsymbol{A}$, and $\sum \bar{\boldsymbol{B}}_i = \boldsymbol{B}_1$. When analytical equations are available, the selection of $\boldsymbol{f}_i, i \in \mathcal{N}_{n_p}$ can be made such that each Δ_i is dependent on the least number of states and inputs, allowing for tighter linear bounds on the nonlinearity (e.g., $\boldsymbol{f}_i = \boldsymbol{1}_i^{\mathsf{T}}\boldsymbol{f}$). The use of too many n_p, however, runs the risk of untangling favorable cancellation and being more computationally difficult to solve. Otherwise, if experimental data, such as drag coefficients from wind tunnel testing, or numerical data, such as lift coefficients from CFD simulations, are available, they can be similarly incorporated as input–output data points of $\Delta_i, i \in \mathcal{N}_{n_p}$. The samples are often performed to span a grid space of sufficiently small interval and may be appended to approximate the dynamics as needed. Furthermore, it is assumed that knowledge of an equilibrium point $\boldsymbol{x}_0$ and $\boldsymbol{u}_0$ as well as the linearized model $\boldsymbol{A}$ and $\boldsymbol{B}_1$ is available, which can be obtained through system identification during small-amplitude flight tests, as demonstrated in [24].

Assuming that a full-state measurement is available, a static full-state feedback controller of $\delta\boldsymbol{u} = \boldsymbol{K}\delta\boldsymbol{x}$ is chosen. The closed-loop equations can be written, without approximation, by substituting $\delta\boldsymbol{u} = \boldsymbol{K}\delta\boldsymbol{x}$ into Eqs. (2), (3), and (4), yielding

$$\delta\dot{\boldsymbol{x}} = (\boldsymbol{A} + \boldsymbol{B}_1\boldsymbol{K})\delta\boldsymbol{x} + \boldsymbol{B}_2\boldsymbol{p} \tag{9}$$

$$p_i = \Delta_i(\boldsymbol{v}_i),\ i \in \mathcal{N}_{n_p} \tag{10}$$

$$\boldsymbol{v}_i = \boldsymbol{E}_i(\boldsymbol{C}_i\delta\boldsymbol{x} + \boldsymbol{D}_i\boldsymbol{K}\delta\boldsymbol{x}),\ i \in \mathcal{N}_{n_p} \tag{11}$$

A block diagram illustrating the closed-loop system (9)–(–11) is shown in Fig. 1a, where Eqs. (9) and (11) represent a state-space realization for $\boldsymbol{G}$ in Fig. 1a, while Eq. (10) represents $\boldsymbol{\Delta}$ in Fig. 1a.

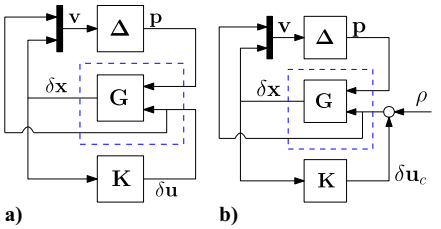

Fig. 1 Block diagrams of a) the closed-loop nonlinear system and b) the closed-loop nonlinear system with an exogenous input ρ.

The objective of this paper is to synthesize a static full-state feedback controller $\boldsymbol{K}$ for a system whose nonlinearities have input and state dependencies such as in Eqs. (9–11). The system is deemed to have input and state dependencies because $\boldsymbol{v}_i$ is composed of both states $\delta\boldsymbol{x}$ and inputs $\delta\boldsymbol{u} = \boldsymbol{K}\delta\boldsymbol{x}$. Furthermore, the synthesized controller is to guarantee boundedness of the system states $\boldsymbol{x}$ within a prescribed region $\mathcal{E}_n(\boldsymbol{E})$ given input–output sampled bounds on the system nonlinearities $\boldsymbol{\Delta}$. To accommodate an excitation signal, the controller additionally has to perform in the presence of a known exogenous input $\rho(t)$ that is oftentimes the known sum of multiple harmonic sine waves of different frequencies and phases. The system input signal is modeled as

$$\delta\boldsymbol{u} = \boldsymbol{K}\delta\boldsymbol{x} + \boldsymbol{B}_3\rho \tag{12}$$

where $\boldsymbol{B}_3$ distributes the input excitation signal to the control inputs. In this paper, only a single exogenous signal is considered, although modifications may be made to account for additional independent signals. The following section presents three options on how to account for the presence of the excitation input to assist in the development of the proposed control synthesis approach.

III. System Model with an Exogenous Input Signal

The known exogenous signal is accounted for using three different approaches when synthesizing a controller to bound the system's closed-loop response. Firstly, a general approach is developed that only assumes that the exogenous input $\rho(t)$ has a maximum magnitude of ψ. This approach is often taken in robust control literature when accounting for unknown exogenous signals [26]. Secondly, by knowing the frequency content and maximum amplitude ψ of the exogenous input, the bandwidth of the signal is captured using a band-pass filter $\boldsymbol{G}_f$ to reflect the absence of low- and high-frequency signals from the control design and analysis. Thirdly, in the case where the exogenous signal is composed of harmonics, the signal can be captured using states that are appended to the original system dynamics. This third option provides the most explicit description of the exogenous signal but suffers from larger computational costs and is only applicable to harmonic exogenous signals.

A. Model with General External Signal

The exogenous input signal ρ in Eq. (12) may be appended to Eqs. (2–4) to yield the following system equations:

$$\delta\dot{\boldsymbol{x}} = (\boldsymbol{A} + \boldsymbol{B}_1\boldsymbol{K})\delta\boldsymbol{x} + \boldsymbol{B}_2\boldsymbol{p} + \boldsymbol{B}_1\boldsymbol{B}_3\rho \tag{13}$$

$$p_i = \Delta_i(\boldsymbol{v}_i),\ i \in \mathcal{N}_{n_p} \tag{14}$$

$$\boldsymbol{v}_i = \boldsymbol{E}_i(\boldsymbol{C}_i + \boldsymbol{D}_i\boldsymbol{K})\delta\boldsymbol{x} + \boldsymbol{E}_i\boldsymbol{D}_i\boldsymbol{B}_3\rho \tag{15}$$

The system is captured in the block diagram Fig. 1b. While the exogenous signal ρ has fixed amplitude of ψ, the frequency content is not restricted here. This is the baseline robust control setup.

B. Model with Filtered External Signal

The external signal may be constrained to only contain frequency content that is consistent with a band-pass filter of transfer function $\boldsymbol{G}_f$ with state space representation of $(\boldsymbol{A}_f, \boldsymbol{B}_f, \boldsymbol{C}_f, \boldsymbol{0})$ of input ρ and output ν, where ν becomes the filtered input into the system described in Sec. III.A. The filter $\boldsymbol{G}_f$ encompasses the frequency content of the expected signal and has gains exceeding 1 at these frequencies. A band-pass filter may be incorporated for such purpose with the state-space realization

$$\dot{\boldsymbol{x}}_f = \boldsymbol{A}_f\boldsymbol{x}_f + \boldsymbol{B}_f\rho \tag{16}$$

$$\nu = \boldsymbol{C}_f\boldsymbol{x}_f \tag{17}$$

With the addition of the controller, the perturbed input is $\delta\boldsymbol{u} = \boldsymbol{K}\delta\boldsymbol{x} + \boldsymbol{B}_3\nu$. The system can be generalized with the states $\boldsymbol{y}^{\mathsf{T}} = [\delta\boldsymbol{x}^{\mathsf{T}}\boldsymbol{x}_f^{\mathsf{T}}]$ as

$$\dot{\boldsymbol{y}} = \begin{bmatrix} \boldsymbol{A} + \boldsymbol{B}_1\boldsymbol{K} & \boldsymbol{B}_1\boldsymbol{B}_3\boldsymbol{C}_f \\ \boldsymbol{0} & \boldsymbol{A}_f \end{bmatrix}\boldsymbol{y} + \begin{bmatrix} \boldsymbol{B}_2 \\ \boldsymbol{0} \end{bmatrix}\boldsymbol{p} + \begin{bmatrix} \boldsymbol{0} \\ \boldsymbol{B}_f \end{bmatrix}\rho \tag{18}$$

$$= \left(\begin{bmatrix} \boldsymbol{A} & \boldsymbol{B}_1\boldsymbol{B}_3\boldsymbol{C}_f \\ \boldsymbol{0} & \boldsymbol{A}_f \end{bmatrix} + \begin{bmatrix} \boldsymbol{B}_1\boldsymbol{K} & \boldsymbol{0} \\ \boldsymbol{0} & \boldsymbol{0} \end{bmatrix}\right)\boldsymbol{y} + \begin{bmatrix} \boldsymbol{B}_2 \\ \boldsymbol{0} \end{bmatrix}\boldsymbol{p} + \begin{bmatrix} \boldsymbol{0} \\ \boldsymbol{B}_f \end{bmatrix}\rho \tag{19}$$

$$= (\boldsymbol{A}_b + \boldsymbol{A}_k)\boldsymbol{y} + \hat{\boldsymbol{B}}_2\boldsymbol{p} + \hat{\boldsymbol{B}}_f\rho \tag{20}$$

where the matrices $\boldsymbol{A}_b = \begin{bmatrix} \boldsymbol{A} & \boldsymbol{B}_1\boldsymbol{B}_3\boldsymbol{C}_f \\ \boldsymbol{0} & \boldsymbol{A}_f \end{bmatrix}$ and $\boldsymbol{A}_k = \begin{bmatrix} \boldsymbol{B}_1\boldsymbol{K} & \boldsymbol{0} \\ \boldsymbol{0} & \boldsymbol{0} \end{bmatrix}$ are defined to separate the portions of the dynamics that depend on the control gain $\boldsymbol{K}$ from those that do not.

The closed-loop equations of motion with the band-pass filter representation of excitation input are described by

$$\dot{\boldsymbol{y}} = (\boldsymbol{A}_b + \boldsymbol{A}_k)\boldsymbol{y} + \hat{\boldsymbol{B}}_2\boldsymbol{p} + \hat{\boldsymbol{B}}_f\rho \tag{21}$$

$$p_i = \Delta_i(\boldsymbol{v}_i), i \in \mathcal{N}_{n_p} \tag{22}$$

$$\boldsymbol{v}_i = \boldsymbol{E}_i(\boldsymbol{C}_i + \boldsymbol{D}_i\boldsymbol{K})\delta\boldsymbol{x} + \boldsymbol{E}_i\boldsymbol{D}_i\boldsymbol{C}_f\boldsymbol{x}_f \tag{23}$$

It is worth noting that the band-pass filter described in this section is only to be used as a model to improve knowledge of the exogenous excitation signal for the controller synthesis method outlined in Sec. IV.C. During flight test implementation, the actual exogenous excitation signal would be applied directly to the system without the band-pass filter.

C. Model with Harmonic Excitation Signal

The approach taken in this section involves modeling the harmonic signal through the use of appended states to the original state space. Each harmonic excitation signal is represented as the free-response output of a two-state state-space system. For example, the signal $h_1(t) = A_1\sin(\omega_1 + \phi_1)$ corresponds to the solution of the ordinary differential equation $\ddot{h}_1 + 2\mu\omega_1\dot{h}_1 + \omega_1^2 h_1 = 0$, where $\mu = 0$ and the initial condition $\boldsymbol{\beta}_1(0)$ is chosen appropriately to match the amplitude and phase of the harmonic signal. This corresponds to the output of the state-space system

$$\dot{\boldsymbol{\beta}}_1 = \begin{bmatrix} 0 & 1 \\ -\omega_1^2 & -2\mu\omega_1 \end{bmatrix}\boldsymbol{\beta}_1 \tag{24}$$

$$h_1 = \begin{bmatrix} 1 & 0 \end{bmatrix}\boldsymbol{\beta}_1 \tag{25}$$

In this work, a small amount of decay or damping in the harmonic signal is introduced through the parameter $\mu > 0$ to aid with numerical computations. This damping value can be made very small to minimize the effects on the actual harmonic signal, especially for the first few cycles when flight testing is performed. For compactness in subsequent derivations, Eqs. (24) and (25) are expressed as

$$\dot{\boldsymbol{\beta}}_1 = \boldsymbol{S}_1\boldsymbol{\beta}_1 \tag{26}$$

$$h_1 = \boldsymbol{T}_1\boldsymbol{\beta}_1 \tag{27}$$

Consider a signal formed by the summation of n_h harmonic signals given by

$$h(t) = A_1\sin(\omega_1 t + \phi_1) + A_2\sin(\omega_2 t + \phi_2) + \cdots + A_{n_h}\sin(\omega_{n_h} t + \phi_{n_h}) \tag{28}$$

This signal h can be generated as the output of the state-space system

$$\dot{\boldsymbol{\beta}} = \boldsymbol{S}\boldsymbol{\beta} \tag{29}$$

$$h = \boldsymbol{T}\boldsymbol{\beta} \tag{30}$$

where $\boldsymbol{S} = \mathrm{diag}(\boldsymbol{S}_1, \boldsymbol{S}_2, \ldots, \boldsymbol{S}_{n_h})$, $\boldsymbol{T} = [\boldsymbol{T}_1 \ \cdots \ \boldsymbol{T}_{n_h}]$, and $\boldsymbol{\beta} = [\boldsymbol{\beta}_1^\mathsf{T} \ \cdots \ \boldsymbol{\beta}_{n_h}^\mathsf{T}]^\mathsf{T}$. The state-space representations of $\boldsymbol{S}$ and $\boldsymbol{T}$ are not unique. A change of variable of $\bar{\boldsymbol{\beta}} = \boldsymbol{\Pi}\boldsymbol{\beta}$ is introduced as a means to improve numerical conditioning and weigh the effects of initial conditions that will be useful later in the control synthesis. The transformed state-space system is

$$\dot{\bar{\boldsymbol{\beta}}} = \bar{\boldsymbol{S}}\bar{\boldsymbol{\beta}} \tag{31}$$

$$h = \bar{\boldsymbol{T}}\bar{\boldsymbol{\beta}} \tag{32}$$

where $\bar{\boldsymbol{S}} = \boldsymbol{\Pi}\boldsymbol{S}\boldsymbol{\Pi}^{-1}$ and $\bar{\boldsymbol{T}} = \boldsymbol{T}\boldsymbol{\Pi}^{-1}$.

The control input to the nonlinear hypersonic model described by Eqs. (2–4) is augmented with the harmonic excitation signal $\boldsymbol{B}_3 h$ as

$$\delta\boldsymbol{u} = \boldsymbol{K}\delta\boldsymbol{x} + \boldsymbol{B}_3 h = \boldsymbol{K}\delta\boldsymbol{x} + \boldsymbol{B}_3\bar{\boldsymbol{T}}\bar{\boldsymbol{\beta}} \tag{33}$$

The equation of motion in Eq. (2) can thus be rewritten as

$$\delta\dot{\boldsymbol{x}} = (\boldsymbol{A} + \boldsymbol{B}_1\boldsymbol{K})\delta\boldsymbol{x} + \boldsymbol{B}_2\boldsymbol{p} + \boldsymbol{B}_1\boldsymbol{B}_3\bar{\boldsymbol{T}}\bar{\boldsymbol{\beta}} \tag{34}$$

Augmenting the state vector to include the harmonic excitation states, the new state becomes $\boldsymbol{z}^\mathsf{T} = [\delta\boldsymbol{x}^\mathsf{T} \ \bar{\boldsymbol{\beta}}^\mathsf{T}]$, which results in the augmented dynamics

$$\dot{\boldsymbol{z}} = \begin{bmatrix} \boldsymbol{A} + \boldsymbol{B}_1\boldsymbol{K} & \boldsymbol{B}_1\boldsymbol{B}_3\bar{\boldsymbol{T}} \\ \boldsymbol{0} & \bar{\boldsymbol{S}} \end{bmatrix}\boldsymbol{z} + \begin{bmatrix} \boldsymbol{B}_2 \\ \boldsymbol{0} \end{bmatrix}\boldsymbol{p} \tag{35}$$

$$= \left(\begin{bmatrix} \boldsymbol{A} & \boldsymbol{B}_1\boldsymbol{B}_3\bar{\boldsymbol{T}} \\ \boldsymbol{0} & \bar{\boldsymbol{S}} \end{bmatrix} + \begin{bmatrix} \boldsymbol{B}_1\boldsymbol{K} & \boldsymbol{0} \\ \boldsymbol{0} & \boldsymbol{0} \end{bmatrix}\right)\boldsymbol{z} + \begin{bmatrix} \boldsymbol{B}_2 \\ \boldsymbol{0} \end{bmatrix}\boldsymbol{p} \tag{36}$$

$$= (\boldsymbol{A}_s + \boldsymbol{A}_k)\boldsymbol{z} + \hat{\boldsymbol{B}}_2\boldsymbol{p} \tag{37}$$

where the matrices $\boldsymbol{A}_s = \begin{bmatrix} \boldsymbol{A} & \boldsymbol{B}_1\boldsymbol{B}_3\bar{\boldsymbol{T}} \\ \boldsymbol{0} & \bar{\boldsymbol{S}} \end{bmatrix}$ and $\boldsymbol{A}_k = \begin{bmatrix} \boldsymbol{B}_1\boldsymbol{K} & \boldsymbol{0} \\ \boldsymbol{0} & \boldsymbol{0} \end{bmatrix}$ are defined to separate the portions of the dynamics that depend on the control gain $\boldsymbol{K}$ from those that do not.

The closed-loop equations of motion with harmonic excitation are described by

$$\dot{\boldsymbol{z}} = (\boldsymbol{A}_s + \boldsymbol{A}_k)\boldsymbol{z} + \hat{\boldsymbol{B}}_2\boldsymbol{p} \tag{38}$$

$$p_i = \Delta_i(\boldsymbol{v}_i), \ i \in \mathcal{N}_{n_p} \tag{39}$$

$$\boldsymbol{v}_i = \boldsymbol{E}_i\begin{bmatrix} (\boldsymbol{C}_i + \boldsymbol{D}_i\boldsymbol{K}) & \boldsymbol{D}_i\boldsymbol{B}_3\bar{\boldsymbol{T}} \end{bmatrix}\boldsymbol{z}, \ i \in \mathcal{N}_{n_p} \tag{40}$$

IV. Control Synthesis Conditions in the Presence of Exogenous Excitations

The proposed control synthesis method is presented in this section, starting with a description of the LMI conditions derived in [22] that guarantee closed-loop asymptotic stability of an autonomous nonlinear system with norm bounds on the system's nonlinearities. An extension of the result in [22] is then introduced as a means to provide a transient bound on the norm of the state, rather than simply ensuring asymptotic stability. Matrix inequality conditions are then derived to explicitly account for harmonic excitation signals while maintaining bounded outputs.

A. Control Synthesis Without Any Exogenous Signals

The proposed control synthesis method is formulated starting from the stability theorem presented in [22], which is stated as follows.

Theorem IV.1: Consider the closed-loop system described by Eqs. (9–11), where the perturbations satisfy the norm bounds $\|p_i\|_2 \le \gamma_i\|\boldsymbol{v}_i\|_2, i \in \mathcal{N}_{n_p}$. Let $\boldsymbol{W} > 0$ and $r > 0$ be chosen such that

$\mathbb{X}_c = \mathcal{E}_{n_x}(\boldsymbol{W}) \subseteq \mathbb{X}$ and $\mathbb{U}_c = \mathcal{B}_{n_u}(r) \subseteq \mathbb{U}$, respectively. Then, the closed-loop system is locally asymptotically stable in $\mathbb{X}_c$ if there exist $\boldsymbol{P} \in \mathbb{S}^{n_x}$, $\boldsymbol{K} \in \mathbb{R}^{n_u \times n_x}$, $\tau > 0$, and $\lambda_i > 0$, $i \in \mathcal{N}_{n_p}$, such that $\boldsymbol{P} > 0$ and

$$\begin{bmatrix} \boldsymbol{P}(\boldsymbol{A}+\boldsymbol{B}_1\boldsymbol{K}) + (\boldsymbol{A}+\boldsymbol{B}_1\boldsymbol{K})^{\mathsf{T}}\boldsymbol{P} & \boldsymbol{P}\boldsymbol{B}_2 & \boldsymbol{\Theta} \\ \boldsymbol{B}_2^{\mathsf{T}}\boldsymbol{P} & \boldsymbol{\Lambda} & \boldsymbol{0} \\ \boldsymbol{\Theta}^{\mathsf{T}} & \boldsymbol{0} & \boldsymbol{\Xi} \end{bmatrix} < 0 \tag{41}$$

$$\begin{bmatrix} \tau^2\boldsymbol{1} & \boldsymbol{K} \\ \boldsymbol{K}^{\mathsf{T}} & \boldsymbol{W}^{-1}\boldsymbol{W}^{-1} \end{bmatrix} \geq 0 \tag{42}$$

$$\tau \leq r \tag{43}$$

where $\boldsymbol{\Lambda} = -\text{diag}(\lambda_1, \ldots, \lambda_{n_w})$ and $\boldsymbol{\Xi} = -\text{diag}(\lambda_1/\gamma_1^2\boldsymbol{1}, \ldots, \lambda_{n_w}/\gamma_{n_w}^2\boldsymbol{1})$, $\boldsymbol{\Theta} = [\lambda_1\boldsymbol{\Phi}_1, \ldots, \lambda_n\boldsymbol{\Phi}_{n_w}]$, with $\boldsymbol{\Phi}_i = \boldsymbol{C}_i^{\mathsf{T}} + \boldsymbol{K}^{\mathsf{T}}\boldsymbol{D}_i^{\mathsf{T}}$, $i \in \mathcal{N}_{n_p}$.

Proof: See the proof of Theorem 3.1 in [22]. □

Theorem IV.1 provides a means to certify the asymptotic stability of an autonomous nonlinear system within a local region. Although this was shown to yield a useful control synthesis method for sampled nonlinear systems in [22], it does not provide any guarantees of what might occur to the closed-loop system state during the system's transient response. For example, the state may exit the sampled region $\mathcal{E}(\boldsymbol{W})$ for a period of time before returning and asymptotically stabilizing to the equilibrium point. To overcome the limitation of Theorem IV.1, transient bounds of the states as described in [27,(28, Chap. 6)] are imposed to avoid exceeding the sampled region $\mathcal{E}(\boldsymbol{W})$. Including the weighting matrix $\boldsymbol{W}$, a slight modification of the transient bounds is described in the following lemma for completeness.

Lemma IV.1: Consider the closed-loop system described by Eqs. (9–11), where the perturbations satisfy the norm bounds $\|p_i\|_2 \leq \gamma_i\|\boldsymbol{v}_i\|_2$, $i \in \mathcal{N}_{n_p}$. The transient norm bound

$$\|\boldsymbol{W}^{-1}\delta\boldsymbol{x}(T)\|_2 \leq \xi\|\boldsymbol{W}^{-1}\delta\boldsymbol{x}(0)\|_2 \tag{44}$$

is satisfied if there exist $\boldsymbol{P} \in \mathbb{S}^{n_x}$ and $\xi \in \mathbb{R}_{>0}$ such that $\boldsymbol{P} > 0$, Eq. (41), and

$$\xi\boldsymbol{1} - \boldsymbol{W}^{\mathsf{T}}\boldsymbol{P}\boldsymbol{W} \geq 0 \tag{45}$$

$$\begin{bmatrix} \boldsymbol{W}^{\mathsf{T}}\boldsymbol{P}\boldsymbol{W} & \boldsymbol{1} \\ \boldsymbol{1} & \xi\boldsymbol{1} \end{bmatrix} \geq 0 \tag{46}$$

Proof: The non-negative function $V = \delta\boldsymbol{x}^{\mathsf{T}}\boldsymbol{P}\delta\boldsymbol{x}$ is defined and the proof of Theorem 3.1 in [22] is used with Eq. (41) to show that $\dot{V} \leq 0$. Integrating both sides from $t = 0$ to $t = T$, where $T \in \mathbb{R}_{>0}$, yields $V(T) \leq V(0)$ or $\delta\boldsymbol{x}^{\mathsf{T}}(T)\boldsymbol{P}\delta\boldsymbol{x}(T) \leq \delta\boldsymbol{x}^{\mathsf{T}}(0)\boldsymbol{P}\delta\boldsymbol{x}(0)$. The inequality in Eq. (45) can be rewritten as $\boldsymbol{P} \leq \xi\boldsymbol{W}^{-\mathsf{T}}\boldsymbol{W}^{-1}$. Applying the non-strict Schur complement ([28] p. 28, Chap. 2) to Eq. (46) results in $\boldsymbol{P} \geq \xi^{-1}\boldsymbol{W}^{-\mathsf{T}}\boldsymbol{W}^{-1}$. Combining these results yields

$$\begin{aligned} \xi^{-1}\delta\boldsymbol{x}^{\mathsf{T}}(T)\boldsymbol{W}^{-\mathsf{T}}\boldsymbol{W}^{-1}\delta\boldsymbol{x}(T) &\leq \delta\boldsymbol{x}^{\mathsf{T}}(T)\boldsymbol{P}\delta\boldsymbol{x}(T) \\ &\leq \delta\boldsymbol{x}^{\mathsf{T}}(0)\boldsymbol{P}\delta\boldsymbol{x}(0) \leq \xi\delta\boldsymbol{x}^{\mathsf{T}}(0)\boldsymbol{W}^{-\mathsf{T}}\boldsymbol{W}^{-1}\delta\boldsymbol{x}(0) \end{aligned} \tag{47}$$

or $\xi^{-1}\|\boldsymbol{W}^{-1}\delta\boldsymbol{x}(T)\|_2^2 \leq \xi\|\boldsymbol{W}^{-1}\delta\boldsymbol{x}\|_2^2$. Multiplying both sides of the inequality by ξ and taking the square root of the resulting expression completes the proof. □

This Lemma may be viewed as an extension of Theorem IV.1 such that with a given $\boldsymbol{K}$, $\boldsymbol{W}$, γ_i, $i \in \mathcal{N}_{n_p}$, the transient bound ξ may be minimized or enforced by solving an SDP.

B. Control Synthesis with General Exogenous Signal

In addition to the controller input, an exogenous harmonic excitation signal could be perturbing the system. In the robust control literature, this may be viewed as disturbance or noise ρ. Instead of asymptotic stability, state boundedness is shown by combining Theorem IV.1 and Lemma IV.1.

Theorem IV.2: Consider the closed-loop system described by Eqs. (13–15), where the perturbations satisfy the norm bounds $\|p_i\|_2 \leq \gamma_i\|\boldsymbol{v}_i\|_2$, $i \in \mathcal{N}_{n_p}$. Let $\boldsymbol{W} > 0$ and $r > 0$ be chosen such that $\mathbb{X}_c = \mathcal{E}_{n_x}(\boldsymbol{W}) \subseteq \mathbb{X}$ and $\mathbb{U}_c = \mathcal{B}_{n_u}(r) \subseteq \mathbb{U}$, respectively. Then, the harmonic-embedded closed-loop system is locally bounded as

$$\left\|\boldsymbol{W}^{-1}\delta\boldsymbol{x}(T)\right\|_2^2 \leq \xi^2\left(\left\|\boldsymbol{W}^{-1}\delta\boldsymbol{x}(0)\right\|_2^2 + \|\rho\|_{2T}^2\right) \tag{48}$$

if there exist $\boldsymbol{P} \in \mathbb{S}^{n_x}$, $\boldsymbol{K} \in \mathbb{R}^{n_u \times n_x}$, $\tau > 0$, and $\lambda_i > 0$, $i \in \mathcal{N}_{n_p}$, such that $\boldsymbol{P} > 0$ and

$$\begin{bmatrix} \boldsymbol{P}(\boldsymbol{A}+\boldsymbol{B}\boldsymbol{K}) + (\boldsymbol{A}+\boldsymbol{B}\boldsymbol{K})^{\mathsf{T}}\boldsymbol{P} & \boldsymbol{P}\boldsymbol{B}_2 & \boldsymbol{P}\boldsymbol{B}_1\boldsymbol{B}_3 & \boldsymbol{\Theta} \\ \boldsymbol{B}_2^{\mathsf{T}}\boldsymbol{P} & \boldsymbol{\Lambda} & \boldsymbol{0} & \boldsymbol{0} \\ \boldsymbol{B}_3^{\mathsf{T}}\boldsymbol{B}_1^{\mathsf{T}}\boldsymbol{P} & \boldsymbol{0} & -\xi\boldsymbol{1} & \boldsymbol{\Psi} \\ \boldsymbol{\Theta}^{\mathsf{T}} & \boldsymbol{0} & \boldsymbol{\Psi}^{\mathsf{T}} & \boldsymbol{\Xi} \end{bmatrix} < 0 \tag{49}$$

$$\tau + \psi \leq r \tag{50}$$

are satisfied along with Eqs. (42), (45), and (46). The variables are defined as $\boldsymbol{\Lambda} = -\text{diag}(\lambda_1, \ldots, \lambda_{n_w})$ and $\boldsymbol{\Xi} = -\text{diag}(\lambda_1/\gamma_1^2\boldsymbol{1}, \ldots, \lambda_{n_w}/\gamma_{n_w}^2\boldsymbol{1})$, $\boldsymbol{\Theta} = [\lambda_1\boldsymbol{\Phi}_1, \ldots, \lambda_n\boldsymbol{\Phi}_{n_w}]$, with $\boldsymbol{\Phi}_i^{\mathsf{T}} = \boldsymbol{E}_i(\boldsymbol{C}_i + \boldsymbol{D}_i\boldsymbol{K})$, $i \in \mathcal{N}_{n_p}$, and $\boldsymbol{\Psi} = [\lambda_1\boldsymbol{B}_3^{\mathsf{T}}\boldsymbol{D}_i^{\mathsf{T}}, \ldots, \lambda_n\boldsymbol{B}_3^{\mathsf{T}}\boldsymbol{D}_n^{\mathsf{T}}]$. Furthermore, ψ is the $\mathcal{L}_\infty$ norm of $\rho(t)$ that encapsulates the maximum magnitude of the external signal.

Proof: The proof follows Theorem 3.1 in [22] with some modification. As a first step, it is important to ensure that $\delta\boldsymbol{u} = \boldsymbol{K}\delta\boldsymbol{x} + \boldsymbol{B}_3\rho \in \mathbb{U}$ is satisfied. To determine a suitable constraint that ensures this, it is first noted that $\mathbb{X}_c = \mathcal{E}_{n_x}(\boldsymbol{W}) \subseteq \mathbb{X}$ implies $\|\boldsymbol{W}^{-1}\delta\boldsymbol{x}\|_2 \leq 1$ for $\delta\boldsymbol{x} \in \mathbb{X}_c$. The norm of the feedback control input is bounded as

$$\|\boldsymbol{K}\delta\boldsymbol{x}\|_2 = \|\boldsymbol{K}\boldsymbol{W}\boldsymbol{W}^{-1}\delta\boldsymbol{x}\|_2 \tag{51}$$

$$\leq \bar{\sigma}(\boldsymbol{K}\boldsymbol{W})\|\boldsymbol{W}^{-1}\delta\boldsymbol{x}\|_2 \leq \bar{\sigma}(\boldsymbol{K}\boldsymbol{W}) \tag{52}$$

which can be equivalently expressed as $\|\boldsymbol{K}\delta\boldsymbol{x}\|_2 \leq \tau$, where $\tau^2\boldsymbol{1} \geq \boldsymbol{K}\boldsymbol{W}\boldsymbol{W}\boldsymbol{K}^{\mathsf{T}}$. Applying the Schur complement to this matrix inequality results in Eq. (42). Knowing that $\psi \leq \max(|\rho|)$, the control input satisfies $\delta\boldsymbol{u} \in \mathbb{U}$ if $\tau + \psi \leq r$, which is the constraint in Eq. (50).

Defining the non-negative function $V = \delta\boldsymbol{x}^{\mathsf{T}}\boldsymbol{P}\delta\boldsymbol{x}$, $\boldsymbol{P} > 0$, taking its time derivative, and using Eq. (13) yields

$$\dot{V} = \begin{bmatrix} \delta\boldsymbol{x} \\ \boldsymbol{p} \\ \rho \end{bmatrix}^{\mathsf{T}} \begin{bmatrix} \boldsymbol{P}(\boldsymbol{A}+\boldsymbol{B}\boldsymbol{K}) + (\boldsymbol{A}+\boldsymbol{B}\boldsymbol{K})^{\mathsf{T}}\boldsymbol{P} & \boldsymbol{P}\boldsymbol{B}_2 & \boldsymbol{P}\boldsymbol{B}_1\boldsymbol{B}_3 \\ * & \boldsymbol{0} & \boldsymbol{0} \\ * & * & -\xi\boldsymbol{1} \end{bmatrix} \begin{bmatrix} \delta\boldsymbol{x} \\ \boldsymbol{p} \\ \rho \end{bmatrix} + \xi\rho^2 \tag{53}$$

The inputs and outputs of each Δ_i can be rewritten as

$$\begin{bmatrix} \boldsymbol{v} \\ p_i \end{bmatrix} = \begin{bmatrix} \boldsymbol{E}_i(\boldsymbol{C}_i + \boldsymbol{D}_i\boldsymbol{K}) & \boldsymbol{0} & \boldsymbol{D}_i\boldsymbol{B}_3 \\ \boldsymbol{0} & \boldsymbol{1}_i^{\mathsf{T}} & \boldsymbol{0} \end{bmatrix} \begin{bmatrix} \delta\boldsymbol{x} \\ \boldsymbol{p} \\ \rho \end{bmatrix} \tag{54}$$

With knowledge that $p_i^2 \leq \gamma_i^2\|\boldsymbol{v}_i\|_2$ is true pointwise in time for each $\Delta_i, \in \mathcal{N}_{n_p}$, this inequality can be written as

$$\begin{bmatrix} \boldsymbol{v}_i \\ p_i \end{bmatrix}^{\mathsf{T}} \begin{bmatrix} \gamma_i^2 \mathbf{1} & \mathbf{0} \\ \mathbf{0} & -1 \end{bmatrix} \begin{bmatrix} \boldsymbol{v}_i \\ p_i \end{bmatrix} \geq 0 \tag{55}$$

Multiplying both sides of Eq. (55) by Eq. (54) yields

$$\begin{bmatrix} \delta \boldsymbol{x} \\ \boldsymbol{p} \\ \rho \end{bmatrix}^{\mathsf{T}} \begin{bmatrix} \gamma_i^2 \boldsymbol{\Phi}_i \boldsymbol{\Phi}_i^{\mathsf{T}} & \mathbf{0} & \gamma_i^2 \boldsymbol{\Phi}_i \boldsymbol{D}_i \boldsymbol{B}_3 \\ * & -\mathbf{1}_i \mathbf{1}_i^{\mathsf{T}} & \mathbf{0} \\ * & * & \gamma_i^2 \boldsymbol{B}_3^{\mathsf{T}} \boldsymbol{D}_i^{\mathsf{T}} \boldsymbol{D}_i \boldsymbol{B}_3 \end{bmatrix} \begin{bmatrix} \delta \boldsymbol{x} \\ \boldsymbol{p} \\ \rho \end{bmatrix} \geq 0 \tag{56}$$

Applying the Schur complement to Eq. (49) results in

$$\begin{bmatrix} \boldsymbol{P}(\boldsymbol{A}+\boldsymbol{B}\boldsymbol{K}) + (\boldsymbol{A}+\boldsymbol{B}\boldsymbol{K})^{\mathsf{T}}\boldsymbol{P} & \boldsymbol{P}\boldsymbol{B}_2 & \boldsymbol{P}\boldsymbol{B}_1\boldsymbol{B}_3 \\ \boldsymbol{B}_2^{\mathsf{T}}\boldsymbol{P} & \boldsymbol{\Lambda} & \mathbf{0} \\ \boldsymbol{B}_3^{\mathsf{T}}\boldsymbol{B}_2^{\mathsf{T}}\boldsymbol{P} & \mathbf{0} & -\xi\mathbf{1} \end{bmatrix} - \begin{bmatrix} \boldsymbol{\Theta} \\ \mathbf{0} \\ \boldsymbol{\Psi} \end{bmatrix} \boldsymbol{\Xi}^{-1} \begin{bmatrix} \boldsymbol{\Theta} \\ \mathbf{0} \\ \boldsymbol{\Psi} \end{bmatrix}^{\mathsf{T}} < 0 \tag{57}$$

which can be equivalently written as

$$\begin{bmatrix} \boldsymbol{P}(\boldsymbol{A}+\boldsymbol{B}\boldsymbol{K}) + (\boldsymbol{A}+\boldsymbol{B}\boldsymbol{K})^{\mathsf{T}}\boldsymbol{P} & \boldsymbol{P}\boldsymbol{B}_2 & \boldsymbol{P}\boldsymbol{B}_1\boldsymbol{B}_3 \\ \boldsymbol{B}_2^{\mathsf{T}}\boldsymbol{P} & \boldsymbol{\Lambda} & \mathbf{0} \\ \boldsymbol{B}_3^{\mathsf{T}}\boldsymbol{B}_2^{\mathsf{T}}\boldsymbol{P} & \mathbf{0} & -\xi\mathbf{1} \end{bmatrix} - \sum_{i=1}^{n_p} \lambda_i \begin{bmatrix} \boldsymbol{\Phi}_i \\ \mathbf{0} \\ \boldsymbol{B}_3^{\mathsf{T}}\boldsymbol{D}_i^{\mathsf{T}} \end{bmatrix} \frac{\gamma_i^2}{\lambda_i} \mathbf{1} \begin{bmatrix} \boldsymbol{\Phi}_i \\ \mathbf{0} \\ \boldsymbol{B}_3^{\mathsf{T}}\boldsymbol{D}_i^{\mathsf{T}} \end{bmatrix}^{\mathsf{T}} \lambda_i < 0 \tag{58}$$

Multiplying Eq. (58) on the left and right by $[\,\delta\boldsymbol{x}^{\mathsf{T}} \quad \boldsymbol{p}^{\mathsf{T}} \quad \rho\,]$ and $[\,\delta\boldsymbol{x}^{\mathsf{T}} \quad \boldsymbol{p}^{\mathsf{T}} \quad \rho\,]^{\mathsf{T}}$ and then substituting in Eq. (53) results in

$$\dot{V} - \xi\rho^2 + \sum_{i=1}^{n_p} \lambda_i \begin{bmatrix} \delta \boldsymbol{x} \\ \boldsymbol{p} \\ \rho \end{bmatrix}^{\mathsf{T}} \begin{bmatrix} \gamma_i^2 \boldsymbol{\Phi}_i \boldsymbol{\Phi}_i^{\mathsf{T}} & \mathbf{0} & \gamma_i^2 \boldsymbol{\Phi}_i \boldsymbol{D}_i \boldsymbol{B}_3 \\ * & -\mathbf{1}_i \mathbf{1}_i^{\mathsf{T}} & \mathbf{0} \\ * & * & \gamma_i^2 \boldsymbol{B}_3^{\mathsf{T}} \boldsymbol{D}_i^{\mathsf{T}} \boldsymbol{D}_i \boldsymbol{B}_3 \end{bmatrix} \begin{bmatrix} \delta \boldsymbol{x} \\ \boldsymbol{p} \\ \rho \end{bmatrix} < 0 \tag{59}$$

Knowing that $\lambda_i > 0,\ i \in \mathcal{N}_{n_p}$, and Eq. (56) are satisfied, the S-procedure [28, Chap. 2] implies $\dot{V} < \xi\rho^2$. Integrating $\dot{V} < \xi\rho^2$ from $t = 0$ to $t = T$, where $T \in \mathbb{R}_{>0}$, yields $V(T) - V(0) < \xi\int_0^T \rho^2 \mathrm{d}t$. Applying the nonstrict Schur complement, Eq. (46) can be rewritten as $\xi^{-1}\boldsymbol{W}^{-\mathsf{T}}\boldsymbol{W}^{-1} \leq \boldsymbol{P}$. The constraint (45) can be rewritten as $\boldsymbol{P} \leq \xi\boldsymbol{W}^{-\mathsf{T}}\boldsymbol{W}^{-1}$. Combining these results yields

$$\begin{aligned} \xi^{-1}\delta\boldsymbol{x}(T)^{\mathsf{T}}\boldsymbol{W}^{-\mathsf{T}}\boldsymbol{W}^{-1}\delta\boldsymbol{x}(T) \leq \delta\boldsymbol{x}(T)^{\mathsf{T}}\boldsymbol{P}\delta\boldsymbol{x}(T) \leq \delta\boldsymbol{x}(0)^{\mathsf{T}}\boldsymbol{P}\delta\boldsymbol{x}(0) \\ + \xi\int_0^T \rho^2 \,\mathrm{d}t \leq \xi\boldsymbol{x}(0)^{\mathsf{T}}\boldsymbol{W}^{-\mathsf{T}}\boldsymbol{W}^{-1}\boldsymbol{x}(0) + \xi\int_0^T \rho^2 \,\mathrm{d}t \end{aligned} \tag{60}$$

Multiplying by ξ and using both ends of the inequalities results in

$$\left\|\boldsymbol{W}^{-1}\delta\boldsymbol{x}(T)\right\|_2^2 \leq \xi^2\left(\left\|\boldsymbol{W}^{-1}\delta\boldsymbol{x}(0)\right\|_2^2 + \left\|\rho\right\|_{2T}^2\right) \tag{61}$$

which completes the proof. □

C. Control Synthesis with Filtered Exogenous Signal

The control synthesis with a general exogenous signal presented in Sec. IV.B does not take advantage of any knowledge of the known frequency content of the signal. To do so, a band-pass filter may be incorporated within the analysis that filters out frequencies that are not present within the excitation inputs. The additional filter states are accounted for within the following theorem.

Theorem IV.3: Consider the closed-loop system described by Eqs. (21), (22), and (23), where the perturbations satisfy the norm bounds $\|p_i\|_2 \leq \gamma_i\|\boldsymbol{v}_i\|_2,\ i \in \mathcal{N}_{n_p}$. Let $\boldsymbol{W} > 0$ and $r > 0$ be chosen such that $\mathbb{X}_c = \mathcal{E}_{n_x}(\boldsymbol{W}) \subseteq \mathbb{X}$ and $\mathbb{U}_c = \mathcal{B}_{n_u}(r) \subseteq \mathbb{U}$, respectively. Then, the harmonic-embedded closed-loop system is locally bounded as

$$\left\|\boldsymbol{W}^{-1}\delta\boldsymbol{x}(T)\right\|_2^2 \leq \xi^2\left(\left\|\boldsymbol{W}^{-1}\delta\boldsymbol{x}(0)\right\|_2^2 + \left\|\rho\right\|_{2\,T}^2\right) \tag{62}$$

if there exist $\boldsymbol{P} \in \mathbb{S}^{n_x}$, $\boldsymbol{K} \in \mathbb{R}^{n_u \times n_x}$, $\tau > 0$, and $\lambda_i > 0,\ i \in \mathcal{N}_{n_p}$, such that $\boldsymbol{P} > 0$ and

$$\begin{bmatrix} \boldsymbol{P}\boldsymbol{A}_b + \boldsymbol{A}_b^{\mathsf{T}}\boldsymbol{P} + \boldsymbol{P}\boldsymbol{A}_k + \boldsymbol{A}_k^{\mathsf{T}}\boldsymbol{P} & \boldsymbol{P}\hat{\boldsymbol{B}}_2 & \boldsymbol{P}\hat{\boldsymbol{B}}_f & \boldsymbol{\Theta} \\ * & \boldsymbol{\Lambda} & \mathbf{0} & \mathbf{0} \\ * & * & -\zeta & \mathbf{0} \\ * & * & * & \boldsymbol{\Xi} \end{bmatrix} < 0 \tag{63}$$

$$\tau + \psi \leq r \tag{64}$$

$$\begin{bmatrix} \bar{\boldsymbol{W}}^{\mathsf{T}}\boldsymbol{P}\bar{\boldsymbol{W}} & \boldsymbol{C}_s^{\mathsf{T}} \\ * & \xi\mathbf{1} \end{bmatrix} \geq 0 \tag{65}$$

$$\bar{\boldsymbol{W}}^{\mathsf{T}}\boldsymbol{P}\bar{\boldsymbol{W}} - \xi\mathbf{1} \leq 0 \tag{66}$$

along with Eq. (42). The variables are $\boldsymbol{\Lambda} = -\mathrm{diag}(\lambda_1, \ldots, \lambda_{n_w})$, $\boldsymbol{\Xi} = -\mathrm{diag}(\lambda_1/\gamma_1^2\mathbf{1}, \ldots, \lambda_{n_w}/\gamma_{n_w}^2\mathbf{1})$, $\boldsymbol{\Theta} = [\lambda_1\boldsymbol{\Phi}_1, \ldots, \lambda_n\boldsymbol{\Phi}_{n_w}]$, $\bar{\boldsymbol{W}} = \mathrm{diag}(\boldsymbol{W}, \mathbf{1})$, $\boldsymbol{C}_s = [\mathbf{1}_{n_x \times n_x}, \mathbf{0}_{n_x \times n_f}]$, and $\boldsymbol{\Phi}_i^{\mathsf{T}} = \boldsymbol{E}_i[\boldsymbol{C}_i + \boldsymbol{D}_i\boldsymbol{K} \quad \boldsymbol{D}_i\boldsymbol{C}_f]$, $i \in \mathcal{N}_{n_p}$. The variable $\psi = \max(|\rho|)$ encapsulates the maximum magnitude of the external signal.

Proof: The proof follows similarly to the proof of Theorem IV.2 and is presented in Sec. A1 in the Appendix. □

D. Control Synthesis with Harmonic Exogenous Signal

If the exogenous signal additional to the controller inputs is composed of known harmonic signals, which is often the case for system identification testing, the information of the signal can be included in the control synthesis with the following theorem that represents the sum of harmonic signals as augmented states to the system.

Theorem IV.4: Consider the closed-loop system described by Eqs. (38), (39), and (40), where the perturbations satisfy the norm bounds $\|p_i\|_2 \leq \gamma_i\|\boldsymbol{v}_i\|_2,\ i \in \mathcal{N}_{n_p}$. Let $\boldsymbol{W} > 0$ and $r > 0$ be chosen such that $\mathbb{X}_c = \mathcal{E}_{n_x}(\boldsymbol{W}) \subseteq \mathbb{X}$ and $\mathbb{U}_c = \mathcal{B}_{n_u}(r) \subseteq \mathbb{U}$, respectively. Then the harmonic-embedded closed-loop system is locally bounded as

$$\left\|\boldsymbol{W}^{-1}\delta\boldsymbol{x}(T)\right\|_2^2 \leq \xi^2\left(\left\|\boldsymbol{W}^{-1}\delta\boldsymbol{x}(0)\right\|_2^2 + \left\|\bar{\boldsymbol{\beta}}(0)\right\|_2^2\right) \tag{67}$$

if there exist $\boldsymbol{P} \in \mathbb{S}^{n_x}$, $\boldsymbol{K} \in \mathbb{R}^{n_u \times n_x}$, $\tau > 0$, and $\lambda_i > 0,\ i \in \mathcal{N}_{n_p}$, such that $\boldsymbol{P} > 0$ and

$$\begin{bmatrix} \boldsymbol{P}(\boldsymbol{A}_s + \boldsymbol{A}_k) + (\boldsymbol{A}_s + \boldsymbol{A}_k)^{\mathsf{T}}\boldsymbol{P} & \boldsymbol{P}\hat{\boldsymbol{B}}_2 & \boldsymbol{\Theta} \\ \hat{\boldsymbol{B}}_2^{\mathsf{T}}\boldsymbol{P} & \boldsymbol{\Lambda} & \mathbf{0} \\ \boldsymbol{\Theta}^{\mathsf{T}} & \mathbf{0} & \boldsymbol{\Xi} \end{bmatrix} < 0 \tag{68}$$

$$\tau + \psi \leq r \tag{69}$$

$$\begin{bmatrix} \bar{\boldsymbol{W}}^{\mathsf{T}}\boldsymbol{P}\bar{\boldsymbol{W}} & \boldsymbol{C}_s^{\mathsf{T}} \\ * & \xi\mathbf{1} \end{bmatrix} \geq 0 \tag{70}$$

$$\bar{\boldsymbol{W}}^{\mathsf{T}}\boldsymbol{P}\bar{\boldsymbol{W}} - \xi\mathbf{1} \leq 0 \tag{71}$$

as well as Eq. (42). The variables are defined as $\boldsymbol{\Lambda} = -\text{diag}(\lambda_1, \ldots, \lambda_{n_w})$ and $\boldsymbol{\Xi} = -\text{diag}(\lambda_1/\gamma_1^2\mathbf{1}, \ldots, \lambda_{n_w/\gamma_{n_w}^2}\mathbf{1}), \boldsymbol{\Theta} = [\lambda_1\boldsymbol{\Phi}_1, \ldots, \lambda_n\boldsymbol{\Phi}_{n_w}]$, with $\boldsymbol{\Phi}_i^\mathsf{T} = \boldsymbol{E}_i[\boldsymbol{C}_i + \boldsymbol{D}_i\boldsymbol{K}\ \boldsymbol{D}_i\bar{\boldsymbol{T}}]$, $i \in \mathcal{N}_{n_p}$, $\bar{\boldsymbol{W}} = \text{diag}(\boldsymbol{W}, \mathbf{1})$, and $\boldsymbol{C}_s = [\mathbf{1}_{n_x\times n_x}\ \mathbf{0}_{n_x\times 2n_h}]$. The variable $\psi = \max(|h|)$ encapsulates the maximum magnitude of the harmonic wave.

Proof: The proof follows similarly to the proof of Theorem IV.2 and can be found in Sec. A2 in the Appendix. □

The result of Theorems IV.2–IV.4 forms the basis of the proposed control synthesis method. Unfortunately, the constraints of Eqs. (42) and (68–71) cannot be solved as an SDP, as they include bilinear matrix inequalities in the variables $\boldsymbol{P}$, $\boldsymbol{K}$, τ, ξ, and $\lambda_i, i \in \mathcal{N}_{n_p}$. To overcome this, the constraints are reformulated and/or relaxed into convex constraints that can be solved as SDPs for controller synthesis. Section V presents the relaxations needed to formulate the proposed iterative convex control synthesis method.

E. Discussion on Closed-Loop Stability and Transient Bounding Results

Theorems IV.2–IV.4 present matrix inequality conditions that guarantee the closed-loop nonlinear system has a transient response bounded within the region $\mathbb{X}_c$ in the presence of exogenous excitation signals. This type of transient bounding result provides confidence that while energy is being injected into the system via the exogenous excitation signals, the system will remain within a safe envelope in which the norm bounds on the nonlinearities have been characterized. In the case where the exogenous excitation signals are removed and the closed-loop system is autonomous, any controller that meets the conditions outlined in Theorem IV.2, IV.3, or IV.4 is guaranteed to result in an asymptotically stable closed-loop system with the region of attraction $\{\delta\boldsymbol{x} \in \mathbb{R}^{n_x} \mid \|\boldsymbol{W}^{-1}\delta\boldsymbol{x}\|_2\}$. In other words, a controller that satisfies Theorem IV.2, IV.3, or IV.4, also satisfies Theorem IV.1 and Lemma IV.1, which guarantees both the transient bound on the state within the sampling region $\mathbb{X}_c$ and asymptotic stability about the equilibrium point.

V. Control Synthesis Relaxation for LMI Computation

The matrix inequalities in the previous section are LMIs in the design variables $\boldsymbol{P}, \lambda_i, i \in \mathcal{N}_{n_p}$, and ζ, which make them suitable for analysis. The matrix inequalities are, however, bilinear matrix inequalities when considering the controller gain $\boldsymbol{K}$ as the design variable. This section provides reformulations of these conditions that result in the proposed iterative convex-optimization synthesis methods.

A key convex relaxation that is implemented to accommodate the augmented states used in Theorem IV.3, and Theorem IV.4 is the restriction that $\boldsymbol{P}$ be block diagonal (i.e., $\boldsymbol{P} = \text{diag}(\boldsymbol{P}_{11}, \boldsymbol{P}_{22})$, where $\boldsymbol{P}_{11} \in \mathbb{S}^{n_x}$ and $\boldsymbol{P}_{22} \in \mathbb{S}^{2n_h}$). The inverse of $\boldsymbol{P}$ is thus also block diagonal, $\boldsymbol{R} = \boldsymbol{P}^{-1} = \text{diag}(\boldsymbol{R}_{11}, \boldsymbol{R}_{22})$, where $\boldsymbol{R}_{11} = \boldsymbol{P}_{11}^{-1}$ and $\boldsymbol{R}_{22} = \boldsymbol{P}_{22}^{-1}$.

Although this iterative control synthesis algorithm is similar in nature to the control synthesis method presented in [22], two key differences are 1) a guaranteed bound on the norm of the system state that must hold pointwise in time, which ensures that the system does not leave the sampled region of the state space, and 2) exogenous harmonic excitation signals are accounted for by the inclusion of internal harmonic dynamics.

Section V.A first presents a relaxation to the controller size. Next, Sec. V.B presents the general relaxation of control synthesis with general exogenous excitation along with the algorithm to solve it. Sections V.C and V.D follow the same format for filtered and harmonic exogenous excitation.

A. Controller Size Relaxation

As with many LMI-based control synthesis methods, changes of variables and congruence transformations are to be applied to the matrix inequalities presented in Sec. IV to yield a convex synthesis algorithm. This section derives a relaxation on the matrix inequality in Eq. (42) that is needed within all three of the proposed synthesis methods in this paper to be compatible with these changes of variables and congruence transformations. To obtain this relaxation, first, a congruence transformation with $\text{diag}(\mathbf{1}, \boldsymbol{R}_{11})$ is applied to Eq. (42), and the change of variables $\epsilon = \sqrt{\tau}$ and $\boldsymbol{F} = \boldsymbol{K}\boldsymbol{R}_{11}$ are made, yielding

$$\begin{bmatrix} \varepsilon\mathbf{1} & \boldsymbol{F} \\ \boldsymbol{F}^\mathsf{T} & (\boldsymbol{W}^{-1}\boldsymbol{R}_{11})^\mathsf{T}(\boldsymbol{W}^{-1}\boldsymbol{R}_{11}) \end{bmatrix} \geq 0 \tag{72}$$

which is a bilinear matrix inequality with respect to $\boldsymbol{R}_{11}$ that ensures $\bar{\sigma}(\boldsymbol{K}\boldsymbol{W}) \leq \sqrt{\varepsilon}$. Using the completion of squares identity $\boldsymbol{X}^\mathsf{T}\boldsymbol{Y} + \boldsymbol{Y}^\mathsf{T}\boldsymbol{X} \leq \boldsymbol{X}^\mathsf{T}\boldsymbol{X} + \boldsymbol{Y}^\mathsf{T}\boldsymbol{Y}$ for $\boldsymbol{X}, \boldsymbol{Y} \in \mathbb{S}^{n_x}$ [27,29] and setting $\boldsymbol{Y} = \mathbf{1}$, $\boldsymbol{X} = \boldsymbol{W}^{-1}\boldsymbol{R}_{11}$, Eq. (72) is relaxed as an LMI:

$$\begin{bmatrix} \varepsilon\mathbf{1} & \boldsymbol{F} \\ \boldsymbol{F}^\mathsf{T} & (\boldsymbol{W}^{-1}\boldsymbol{R}_{11})^\mathsf{T} + (\boldsymbol{W}^{-1}\boldsymbol{R}_{11}) - \mathbf{1} \end{bmatrix} \geq 0 \tag{73}$$

Alternatively, a different relaxation of the bilinear term $(\boldsymbol{W}^{-1}\boldsymbol{R}_{11})^\mathsf{T}(\boldsymbol{W}^{-1}\boldsymbol{R}_{11})$ for a given $\boldsymbol{R}_{11}$ can be performed by linearizing the bilinear term about a feasible $\boldsymbol{R}_{11_0}$, which is similar to the convex overbounding approach in [30]. This is done by setting $\boldsymbol{X} = \boldsymbol{W}^{-1}\boldsymbol{R}_{11}$ and $\boldsymbol{Y} = \boldsymbol{W}^{-1}\boldsymbol{R}_{11_0}$ within the completion of the squares identity to yield the LMI

$$\begin{bmatrix} \varepsilon\mathbf{1} & \boldsymbol{F} \\ \boldsymbol{F}^\mathsf{T} & \boldsymbol{T}_1 \end{bmatrix} \geq 0 \tag{74}$$

where $\boldsymbol{T}_1 = (\boldsymbol{W}^{-1}\boldsymbol{R}_{11})^\mathsf{T}(\boldsymbol{W}^{-1}\boldsymbol{R}_{11_0}) + (\boldsymbol{W}^{-1}\boldsymbol{R}_{11_0})^\mathsf{T}(\boldsymbol{W}^{-1}\boldsymbol{R}_{11}) - (\boldsymbol{W}^{-1}\boldsymbol{R}_{11_0})^\mathsf{T}(\boldsymbol{W}^{-1}\boldsymbol{R}_{11_0})$.

Finally, to express Eq. (42) in terms of the variables $\boldsymbol{K}$ and $\boldsymbol{P}$, instead of $\boldsymbol{F}$ and $\boldsymbol{R}$, a congruence transformation is performed with $\text{diag}(\mathbf{1}, \boldsymbol{P}_{11})$ and then a Schur complement to obtain

$$\begin{bmatrix} \varepsilon\mathbf{1} & \boldsymbol{K} & \mathbf{0} \\ \boldsymbol{K}^\mathsf{T} & \boldsymbol{T}_2 & \boldsymbol{P}_{11} \\ \mathbf{0} & \boldsymbol{P}_{11} & \boldsymbol{R}_{11_0}^{-1}\boldsymbol{W}\boldsymbol{W}\boldsymbol{R}_{11_0}^{-1} \end{bmatrix} \geq 0 \tag{75}$$

where $\boldsymbol{T}_2 = \boldsymbol{W}^{-1}\boldsymbol{W}^{-1}\boldsymbol{R}_{11_0}\boldsymbol{P}_{11} + \boldsymbol{P}_{11}(\boldsymbol{W}^{-1}\boldsymbol{R}_{11_0})^\mathsf{T}\boldsymbol{W}^{-1}$.

B. Control Synthesis Via Relaxation: General Excitation

The matrix inequalities in Theorem IV.2 are not in the form of an LMI that can be solved without modifications. Some manipulation is necessary to relax the bilinear matrix inequality of Eq. (49) for control synthesis using standard LMI solvers iteratively. A suitable LMI relaxation is first presented, followed by the proposed iterative synthesis method.

1. Relaxation for LMI: General Excitation

Applying a congruence transformation of $\text{diag}(\boldsymbol{R}, \mathbf{1})$ to Eq. (49), where $\boldsymbol{R} = \boldsymbol{P}^{-1}$ and $\boldsymbol{F} = \boldsymbol{K}\boldsymbol{R}$, results in

$$\begin{bmatrix} \boldsymbol{A}\boldsymbol{R} + \boldsymbol{B}\boldsymbol{F} + \boldsymbol{R}\boldsymbol{A}^\mathsf{T} + \boldsymbol{F}^\mathsf{T}\boldsymbol{B}^\mathsf{T} & \boldsymbol{B}_2 & \boldsymbol{B}_1\boldsymbol{B}_3 & \tilde{\boldsymbol{\Theta}} \\ * & \boldsymbol{\Lambda} & \mathbf{0} & \mathbf{0} \\ * & * & -\xi\mathbf{1} & \boldsymbol{\Psi} \\ * & * & * & \boldsymbol{\Xi} \end{bmatrix} > 0 \tag{76}$$

where $\tilde{\boldsymbol{\Theta}} = [\lambda_1\tilde{\boldsymbol{\Phi}}_1 \quad \ldots \quad \lambda_n\tilde{\boldsymbol{\Phi}}_n]$ and $\tilde{\boldsymbol{\Phi}}_i = \boldsymbol{R}\boldsymbol{C}_i^\mathsf{T} + \boldsymbol{F}^\mathsf{T}\boldsymbol{D}_i^\mathsf{T}$.

Next, setting all $\lambda_i = \lambda$ and then applying a congruence transformation of $\text{diag}(\sqrt{\lambda}\mathbf{1}, 1/\sqrt{\lambda}\mathbf{1}, \sqrt{\lambda}\mathbf{1}, 1/\sqrt{\lambda}\mathbf{1})$ and change of variables of $\bar{\boldsymbol{R}} = \lambda\boldsymbol{R}$ and $\bar{\boldsymbol{F}} = \lambda\boldsymbol{F}$ yields

$$\begin{bmatrix} A\bar{R} + B\bar{F} + \bar{R}A^\top + \bar{F}^\top B^\top & B_2 & \lambda B_1 B_3 & \bar{\Theta} \\ * & -\mathbf{1} & \mathbf{0} & \mathbf{0} \\ * & * & -\lambda\xi\mathbf{1} & \Psi \\ * & * & * & \tilde{\Xi} \end{bmatrix} > 0 \quad (77)$$

where $\bar{\Theta} = [\bar{\Phi}_1 \quad \dots \quad \bar{\Phi}_n]$, $\bar{\Phi}_i = \bar{R}C_i^\top + \bar{F}^\top D_i^\top$, and $\tilde{\Xi} = -\text{diag}(1/\gamma_1^2, \dots 1/\gamma_n^2)$.

2. Iterative Control Synthesis Algorithm: General Excitation

Theorem IV.2, along with the relaxations presented in Secs. V.A and V.B, is used to formulate the following iterative controller synthesis method.

1) Initialize W, r, E_i, $i \in \mathcal{N}_{n_p}$, and ξ to compute $\mathbb{X}_c = \mathcal{E}_{n_x}(W) = \{x \in \mathbb{R}^{n_x} | \|W^{-1}x\|_2 \le 1\}$ and $\mathbb{U}_c = \mathcal{B}_{n_u}(r+\psi) = \{u \in \mathbb{R}^{n_u} | \|u\|_2 \le r+\psi\}$. The initialization may be informed by the goals of the controller. For example, $\mathcal{E}_n(W)$ is chosen to encompass the expected initial states, r may be set to the largest allowable actuation, and ξ is set to a value larger than 1 (e.g., $\xi = 4$).

2) Compute samples $p_i = \Delta_i(x, u)$ for $x \in \mathbb{X}_c$ and $u \in \mathbb{U}_c$ to compute the norm bounds γ_i, $i \in \mathcal{N}_{n_p}$ that satisfy (55).

3) Set γ_i to a very small value and solve for a feasible R, F, and ε that satisfy the constraints (73), (77), $R > 0$, and $\varepsilon > 0$. If no feasible solution is found, return to step 1 to initialize with smaller, scaled-down values of W, r, and/or ξ. Otherwise, set $K = FP$.

4) Set $P_0 = W^{-1}$ and use K to solve for a feasible P, ε, and λ_i, $i \in \mathcal{N}_{n_p}$ subject to constraints (49), (75), $P > 0$, $\varepsilon > 0$, and $\lambda_i > 0$, $i \in \mathcal{N}_{n_p}$. If no feasible solution is found, return to step 1 to initialize with smaller, scaled-down values of W, r, and/or ξ. Otherwise, set $R = P^{-1}$.

5) Fix R_0 and solve for R and ε subject to constraints (74), (76), $R > 0$, and $\varepsilon > 0$ that minimize ε. If no feasible solution is found, return to step 1 to initialize with smaller, scaled-down values of W, r, and/or ξ. Otherwise, set $K = FP$.

6) If the stopping criterion $\tau + \psi \le r$ is met, minimize ξ subject to constraints (45), (46), (49), $P > 0$, and $\lambda_i > 0$, $i \in \mathcal{N}_{n_p}$, and then exit. Otherwise, return to step 4.

The small value of γ_i in step 3 can be viewed as a means of reducing the nonlinearity constraints when solving for a feasible K. Having γ_i match the values in step 2 is equivalent to having all of the nonlinearities accounted for, which might be difficult in the first iteration, and thus a nonzero small value of γ_i will aid finding a solution in step 3.

C. Control Synthesis via Relaxation: Filtered Excitation

The matrix inequalities in Theorem IV.3 are not in the form of LMI that can be solved without modifications. Some manipulation is necessary to relax the bilinear matrix inequality in Eq. (63) for control synthesis using standard LMI solvers iteratively. A suitable LMI relaxation is first presented, followed by the proposed iterative synthesis method.

1. Relaxation for LMI: Filtered Excitation

Applying a congruence transformation of $\text{diag}(P^{-1}, \mathbf{1})$ to Eq. (63), where $R = P^{-1}$ and $F = KR_{11}$, yields

$$\begin{bmatrix} A_bR + RA_b^\top + A_kR + RA_k^\top & \hat{B}_2 & \hat{B}_f & \tilde{\Theta} \\ * & \Lambda & \mathbf{0} & \mathbf{0} \\ * & * & -\xi\mathbf{1} & \mathbf{0} \\ * & * & * & \Xi \end{bmatrix} > 0 \quad (78)$$

where $\tilde{\Theta} = [\lambda_1\tilde{\Phi}_1 \quad \dots \quad \lambda_n\tilde{\Phi}_n]$,

$$\tilde{\Phi}_i = \begin{bmatrix} R_{11}C_i^\top + F^\top D_i^\top \\ R_{22}C_f^\top D_i^\top \end{bmatrix}$$

and

$$A_kR = \begin{bmatrix} BKR_{11} & \mathbf{0} \\ \mathbf{0} & \mathbf{0} \end{bmatrix} = \begin{bmatrix} BF & \mathbf{0} \\ \mathbf{0} & \mathbf{0} \end{bmatrix}$$

.

Further relaxing $\lambda_i = \lambda$ and applying a congruence transformation of $\text{diag}(\sqrt{\lambda}\mathbf{1}, 1/\sqrt{\lambda}\mathbf{1}, \sqrt{\lambda}\mathbf{1}, 1/\sqrt{\lambda})$ yields

$$\begin{bmatrix} \lambda(A_bR + RA_b^\top + A_kR + RA_k^\top & \hat{B}_2 & \lambda\hat{B}_f & \tilde{\Theta} \\ * & \mathbf{1} & \mathbf{0} & \mathbf{0} \\ * & * & -\lambda\xi\mathbf{1} & \mathbf{0} \\ * & * & * & \tilde{\Xi} \end{bmatrix} > 0 \quad (79)$$

where $\tilde{\Xi} = -\text{diag}(1/\gamma_1^2, \dots, 1/\gamma_n^2)$.

With a change of coordinates of $\bar{R} = \lambda R$ and $\bar{F} = \lambda F = K\bar{R}$,

$$\begin{bmatrix} A_b\bar{R} + \bar{R}A_b^\top + A_k\bar{R} + \bar{R}A_k^\top & \hat{B}_2 & \lambda\hat{B}_f & \bar{\Theta} \\ * & \mathbf{1} & \mathbf{0} & \mathbf{0} \\ * & * & -\lambda\xi\mathbf{1} & \mathbf{0} \\ * & * & * & \tilde{\Xi} \end{bmatrix} > 0 \quad (80)$$

where $\bar{\Theta} = [\bar{\Phi}_1 \quad \dots \quad \bar{\Phi}_n]$,

$$\bar{\Phi}_i = \begin{bmatrix} \bar{R}_{11}C_i^\top + \bar{F}^\top D_i^\top \\ \bar{R}_{22}C_f^\top D_i^\top \end{bmatrix}$$

and $A_k\bar{R} = \begin{bmatrix} B\bar{F} & \mathbf{0} \\ \mathbf{0} & \mathbf{0} \end{bmatrix}$.

2. Iterative Control Synthesis Algorithm: Filtered Excitation

Theorem IV.3, along with the relaxations presented in Secs. V.A and V.C, are used to formulate the following iterative controller synthesis method:

1) Initialize W, r, E_i, $i \in \mathcal{N}_{n_p}$, and ξ to compute $\mathbb{X}_c = \mathcal{E}_{n_x}(W) = \{x \in \mathbb{R}^{n_x} | \|W^{-1}x\|_2 \le 1\}$ and $\mathbb{U}_c = \mathcal{B}_{n_u}(r+\psi) = \{u \in \mathbb{R}^{n_u} | \|u\|_2 \le r+\psi\}$. The initialization may be informed by the goals of the controller. For example, $\mathcal{E}_n(W)$ is chosen to encompass the expected initial states, r may be set to the largest allowable actuation, and ξ is set to a value larger than 1 (e.g., $\xi = 4$).

2) Compute samples $p_i = \Delta_i(x, u)$ for $x \in \mathbb{X}_c$ and $u \in \mathbb{U}_c$ to compute the norm bounds γ_i, $i \in \mathcal{N}_{n_p}$ that satisfy Eq. (55).

3) Set γ_i to a very small value and solve for a feasible R, F, and ε that satisfy the constraints (73), (80), $R > 0$, and $\varepsilon > 0$. If no feasible solution is found, return to step 1 to initialize with smaller, scaled-down values of W, r and/or ξ. Otherwise, set $K = FP$.

4) Set $P_0 = \text{diag}(W^{-1}, \mathbf{1})$ and use K to solve for a feasible P, ε, and λ_i, $i \in \mathcal{N}_{n_p}$ subject to constraints (63), (75), $P > 0$, $\varepsilon > 0$, and $\lambda_i > 0$, $i \in \mathcal{N}_{n_p}$. If no feasible solution is found, return to step 1 to initialize with smaller, scaled-down values of W, r, and/or ξ. Otherwise, set $R = P^{-1}$.

5) Fix R_0 and solve for R and ε subject to constraints (74), (79), $R > 0$, and $\varepsilon > 0$ that minimize ε. If no feasible solution is found, return to step 1 to initialize with smaller, scaled-down values of W, r, and/or ξ. Otherwise, set $K = FP_{11}$.

6) If the stopping criterion $\tau + \psi \le r$ is met, minimize ξ subject to constraints (45), (46), (49), $P > 0$, and $\lambda_i > 0$, $i \in \mathcal{N}_{n_p}$, then exit. Otherwise, return to step 4.

The small value of γ_i in step 3 can be viewed as a means of reducing the nonlinearity constraints when solving for a feasible K. Having γ_i match the values in step 2 is equivalent to having all of the nonlinearities accounted for, which might be difficult in the first iteration; thus, a nonzero small value of γ_i will aid finding a solution in step 3.

D. Control Synthesis via Relaxation: Harmonic Excitation

The matrix inequalities in Theorem IV.4 are not in the form of LMI that can be solved without modifications. Some manipulation is necessary to relax the bilinear matrix inequality of Eq. (68) for control synthesis using standard LMI solvers iteratively. A suitable LMI relaxation is first presented, followed by the proposed iterative synthesis method.

1. *Relaxation for LMI: Harmonic Excitation*

Applying a congruence transformation to Eq. (68) with $\mathrm{diag}(\boldsymbol{P}^{-1}, \mathbf{1})$ and then using the change of variables $\boldsymbol{R} = \boldsymbol{P}^{-1}$ and $\boldsymbol{F} = \boldsymbol{K}\boldsymbol{R}_{11}$ yields

$$\begin{bmatrix} \boldsymbol{A}_s\boldsymbol{P}^{-1} + \boldsymbol{P}^{-1}\boldsymbol{A}_s^\top + \boldsymbol{A}_k\boldsymbol{P}^{-1} + \boldsymbol{P}^{-1}\boldsymbol{A}_k^\top & \hat{\boldsymbol{B}}_3 & \boldsymbol{P}^{-1}\boldsymbol{\Theta} \\ * & \boldsymbol{\Lambda} & \mathbf{0} \\ * & * & \boldsymbol{\Xi} \end{bmatrix} < 0 \quad (81)$$

$$\begin{bmatrix} \boldsymbol{A}_s\boldsymbol{R} + \boldsymbol{R}\boldsymbol{A}_s^\top + \boldsymbol{A}_k\boldsymbol{R} + \boldsymbol{R}\boldsymbol{A}_k^\top & \hat{\boldsymbol{B}}_3 & \tilde{\boldsymbol{\Theta}} \\ * & \boldsymbol{\Lambda} & \mathbf{0} \\ * & * & \boldsymbol{\Xi} \end{bmatrix} < 0 \quad (82)$$

where $\tilde{\boldsymbol{\Theta}} = [\lambda_1\tilde{\boldsymbol{\Phi}}_1 \quad \dots \quad \lambda_n\tilde{\boldsymbol{\Phi}}_n]$, $i \in \mathcal{N}_{n_p}$, $\tilde{\boldsymbol{\Phi}}_i^\top = \boldsymbol{E}_i[\boldsymbol{C}_{3,i}\boldsymbol{R}_{11} + \boldsymbol{D}_{3,i}\boldsymbol{F}\boldsymbol{D}_{3,i}\bar{\boldsymbol{T}}\boldsymbol{R}_{22}]$, and $\boldsymbol{A}_k\boldsymbol{R} = \mathrm{diag}(\boldsymbol{B}\boldsymbol{F}, \mathbf{0})$.

Another relaxation is defined by setting $\lambda_i = \lambda$ and applying a congruence transformation of $\mathrm{diag}(\sqrt{\lambda}\mathbf{1}, 1/\sqrt{\lambda})$ as well as the coordinate transformations $\bar{\boldsymbol{R}} = \lambda\boldsymbol{R}$ and $\bar{\boldsymbol{F}} = \lambda\boldsymbol{F} = \boldsymbol{K}\bar{\boldsymbol{R}}_{11}$. This yields

$$\begin{bmatrix} \lambda(\boldsymbol{A}_s\boldsymbol{R} + \boldsymbol{R}\boldsymbol{A}_s^\top + \boldsymbol{A}_k\boldsymbol{R} + \boldsymbol{R}\boldsymbol{A}_k^\top) & \hat{\boldsymbol{B}}_3 & \bar{\boldsymbol{\Theta}} \\ * & \mathbf{1} & \mathbf{0} \\ * & * & \bar{\boldsymbol{\Xi}} \end{bmatrix} < 0 \quad (83)$$

$$\begin{bmatrix} \boldsymbol{A}_s\bar{\boldsymbol{R}} + \bar{\boldsymbol{R}}\boldsymbol{A}_s^\top + \boldsymbol{A}_k\bar{\boldsymbol{R}} + \bar{\boldsymbol{R}}\boldsymbol{A}_k^\top & \hat{\boldsymbol{B}}_3 & \bar{\boldsymbol{\Theta}} \\ * & \mathbf{1} & \mathbf{0} \\ * & * & \bar{\boldsymbol{\Xi}} \end{bmatrix} < 0 \quad (84)$$

where $\bar{\boldsymbol{\Theta}} = [\bar{\boldsymbol{\Phi}}_1 \dots \bar{\boldsymbol{\Phi}}_{n_p}]$, $\bar{\boldsymbol{\Phi}}_i^\top = \boldsymbol{E}_i[\boldsymbol{C}_{3,i}\bar{\boldsymbol{R}}_{11} + \boldsymbol{D}_{3,i}\bar{\boldsymbol{F}}\ \boldsymbol{D}_{3,i}\bar{\boldsymbol{T}}\bar{\boldsymbol{R}}_{22}]$, $\boldsymbol{A}_k\bar{\boldsymbol{R}} = \mathrm{diag}(\boldsymbol{B}\bar{\boldsymbol{F}}, \mathbf{0})$, and $\bar{\boldsymbol{\Xi}} = -\mathrm{diag}(1/\gamma_1^2\mathbf{1}, \dots, 1/\gamma_n^2\mathbf{1})$.

The LMIs of Eqs. (82) and (84) are convex relaxations of the bilinear matrix inequality in Eq. (68) that are used to develop the proposed iterative convex control synthesis method described in Sec. V.D.2. Any solutions to the LMIs of Eqs. (82) and (84) are ensured to satisfy the bilinear matrix inequality of Eq. (68).

2. *Iterative Control Synthesis Algorithm: Harmonic Excitation*

Theorem IV.4, along with the relaxations presented in Secs. V.A and V.D, is used to formulate the following iterative controller synthesis method:

1) Initialize $\boldsymbol{W}$, r, $\boldsymbol{\Pi}$, and $\boldsymbol{E}_i$, $i \in \mathcal{N}_{n_p}$ to compute $\mathbb{X}_c = \mathcal{E}_{n_x}(\boldsymbol{W}) = \{\boldsymbol{x} \in \mathbb{R}^{n_x} | \|\boldsymbol{W}^{-1}\boldsymbol{x}\|_2 \le 1\}$ and $\mathbb{U}_c = \mathcal{B}_{n_u}(r) = \{\boldsymbol{u} \in \mathbb{R}^{n_u} | \|\boldsymbol{u}\|_2 \le r\}$. The initialization may be informed by the goals of the controller. For example, $\mathcal{E}_n(\boldsymbol{W})$ is chosen to encompass the expected initial states, r may be set to the largest allowable actuation, and ξ is set to a value larger than 1 (e.g., $\xi = 4$). Furthermore, $\boldsymbol{\Pi}$ may be initiated as a diagonal matrix of $\boldsymbol{\Pi}_{i,i} = 1/\beta_i^*$, $i = 1, \dots, n_h$, where $\beta_i^* = \sup_t(|\beta_i|)$. Compute $\bar{\boldsymbol{S}}$ and $\bar{\boldsymbol{T}}$ given the frequency and amplitude of the expected harmonic excitation signals.

2) Compute samples $p_i = \Delta_i(\boldsymbol{x}, \boldsymbol{u})$ for $\boldsymbol{x} \in \mathbb{X}_c$ and $\boldsymbol{u} \in \mathbb{U}_c$ to compute the norm bounds γ_i, $i \in \mathcal{N}_{n_p}$ that satisfy Eq. (55).

3) Set γ_i to a very small value and solve for a feasible $\boldsymbol{R}$, $\boldsymbol{F}$, and ε that satisfy the constraints (73), (84), $\boldsymbol{R} > 0$, and $\varepsilon > 0$. If no feasible solution is found, return to step 1 to initialize with smaller, scaled-down values of $\boldsymbol{W}$, r, and/or $\boldsymbol{\Pi}$. Otherwise, set $\boldsymbol{K} = \boldsymbol{F}\boldsymbol{P}_{11}$.

4) Set $\boldsymbol{P}_0 = \mathrm{diag}(\boldsymbol{W}^{-1}, \mathbf{1})$ and use $\boldsymbol{K}$ to solve for a feasible $\boldsymbol{P}$, ε, and λ_i, $i \in \mathcal{N}_{n_p}$ subject to constraints (68), (75), $\boldsymbol{P} > 0$, $\varepsilon > 0$, and $\lambda_i > 0$, $i \in \mathcal{N}_{n_p}$. If no feasible solution is found, return to step 1 to initialize with smaller, scaled-down values of $\boldsymbol{W}$, r, and/or $\boldsymbol{\Pi}$. Otherwise, set $\boldsymbol{R}_0 = \boldsymbol{P}^{-1}$.

5) Fix $\boldsymbol{R}_0$ and solve for $\boldsymbol{R}$ and ε subject to constraints (74), (82), $\boldsymbol{R} > 0$, and $\varepsilon > 0$ that minimize ε. If no feasible solution is found, return to step 1 to initialize with smaller, scaled-down values of $\boldsymbol{W}$, r, and/or $\boldsymbol{\Pi}$. Otherwise, set $\boldsymbol{K} = \boldsymbol{F}\boldsymbol{P}_{11}$.

6) If the stopping criterion $\tau + \psi \le r$ is met, minimize ξ subject to constraints (68), (70), (71), (75), $\boldsymbol{P} > 0$, and $\lambda_i > 0$, $i \in \mathcal{N}_{n_p}$ and then exit. Otherwise, return to step 4.

The small value of γ_i in step 3 can be viewed as a means of reducing the nonlinearity constraints when solving for a feasible $\boldsymbol{K}$. Having γ_i match the values in step 2 is equivalent to having all of the nonlinearities accounted for, which might be difficult in the first iteration; thus, a nonzero small value of γ_i will aid finding a solution in step 3.

VI. Numerical Example with a Two-State Nonlinear Model

Before applying the proposed algorithms on the dynamics of a hypersonic vehicle, we apply them on a simpler two-state nonlinear model that has quadratic and input-state coupling nonlinearities. The purpose of this two-state nonlinear model is to highlight the relative strengths and weaknesses of the three different control synthesis methods based on the different options used to characterize the exogenous excitation signals.

A. Two-State Nonlinear Model Dynamics

This section presents a two-state fluid-inspired problem from [22]. This model is inspired by [31] and has two states x_1 and x_2, as well as one input u.

$$\begin{bmatrix} \dot{x}_1 \\ \dot{x}_2 \end{bmatrix} = \begin{bmatrix} -0.1 & 1 \\ 0 & -0.1 \end{bmatrix}\begin{bmatrix} x_1 \\ x_2 \end{bmatrix} + \begin{bmatrix} 1 \\ 1 \end{bmatrix}u + \begin{bmatrix} x_1x_2 + u^2 \\ x_1^2 - u^2 \end{bmatrix} \quad (85)$$

Note that the control input appears nonlinearly in these system dynamics. This can be expressed in a compact form that captures the nonlinearities expressed around the origin as $\boldsymbol{x}_0 = \mathbf{0}$ and $u_0 = 0$, and thus $\delta\boldsymbol{x} = \boldsymbol{x}$ and $\delta u = u$ as in Eqs. (2–4), where the nonlinearities may be expressed as

$$\boldsymbol{\Delta}(\boldsymbol{x}, u) = \begin{bmatrix} p_1 \\ p_2 \end{bmatrix} = \begin{bmatrix} x_1x_2 + u^2 \\ x_1^2 - u^2 \end{bmatrix} \quad (86)$$

Other associated matrices are

$$\boldsymbol{A} = \begin{bmatrix} -0.1 & 1 \\ 0 & -0.1 \end{bmatrix}, \quad \boldsymbol{B}_1 = \begin{bmatrix} 1 \\ 1 \end{bmatrix}, \quad \boldsymbol{B}_2 = \mathbf{1}\boldsymbol{E}_1 = \boldsymbol{E}_2 = \mathbf{1},$$

$$\boldsymbol{C}_1 = \begin{bmatrix} 1 & 0 & 0 \\ 0 & 1 & 0 \end{bmatrix}^\top, \boldsymbol{C}_2 = \begin{bmatrix} 1 & 0 & 0 \\ 0 & 0 & 0 \end{bmatrix}^\top, \boldsymbol{D}_1 = \boldsymbol{D}_2 = \begin{bmatrix} 0 & 0 & 1 \end{bmatrix}^\top$$

Numerical simulations performed for the fluid-inspired model described in this section are presented here. The trim conditions are at the origin. The sampling region of $\mathbb{X}_c \times \mathbb{U}_c$ is set at $\mathbb{X}_c = \mathcal{B}(2.0833)$, or equivalently $\mathbb{X}_c = \mathcal{E}(\boldsymbol{W})$ with $\boldsymbol{W} = 0.48\mathbf{1}$, in all instances and $\mathbb{U}_c = \mathcal{B}(r)$ with $r = 0.47$.

The external signal ρ is a sum of five harmonic sine waves, each with amplitudes of 0.002 and frequencies of 1–5 rad/s with equal spacing. The phase values of the sine waves are [180° 0° 150° 210° 180°] and $\mu = 0.001$. The superposition of the harmonic sine waves has $\psi = (\max|\rho|) = 0.0049$, as shown in Fig. 2. The $\boldsymbol{\Pi}$ matrix was selected to minimize the $\boldsymbol{\beta}_0$ to have a larger region of allowable initial conditions; thus, $\boldsymbol{\Pi} = 0.07 \cdot \max(\mathrm{diag}(\boldsymbol{\beta}))^{-1} = \mathrm{diag}(35, 35, 35, 17.5, 35, 11.6667, 35, 8.75, 35, 7)$ was selected. In all cases, $\xi = 4$ was initialized for algorithms in Secs. V.B.2 and V.C.2.

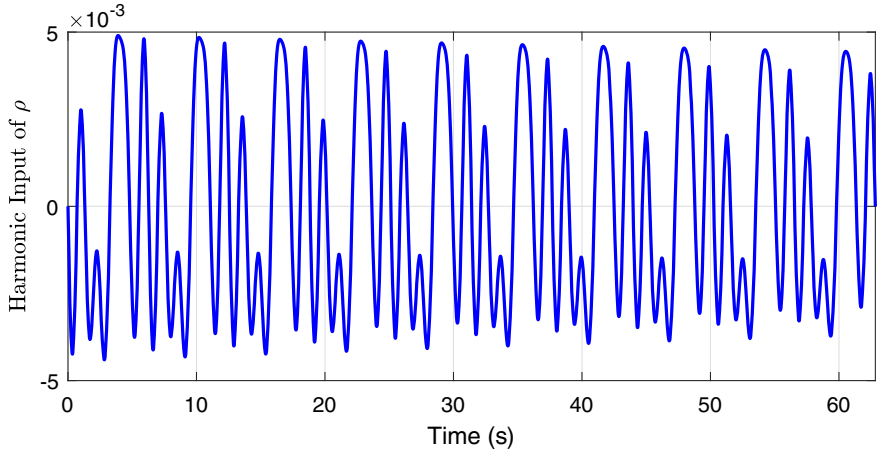

Fig. 2 The harmonic excitation signals ρ applied to the fluid-inspired model in Sec. VI.

B. Numerical Results

The region of attraction of the original two-state nonlinear model without external excitation satisfies Theorem IV.1 with $\|\boldsymbol{x}(0)\|_2 \leq 0.48$. To further satisfy the transient bounds of the sampling region of Lemma IV.1 to ensure that the norm-bound constraints are satisfied, $\xi = 1.2467$ was obtained with no other excitation, giving a region of attraction of $\|\boldsymbol{x}(0)\|_2 \leq 0.385$.

When a general excitation ϕ is introduced, the implementation of the algorithm in Sec. V.B.2 that satisfies Theorem IV.2 yields $\xi = 5.4953$ with a corresponding allowable initial condition $\|\boldsymbol{x}(0)\|_2 \leq 0.0873$ when $\|\rho\|_{2T} = 0$. As time progresses, $\|\rho\|_{2T}$ increases, as observed in Fig. 3, as more energy is being introduced by the exogenous signal. This causes the allowable initial conditions to shrink since the $\|\rho\|_{2T}$ term of the inequality in Eqs. (48) and (62) increases with time.

To further expand the bounded region of the allowable initial condition, the control synthesis using a band-pass filter $\boldsymbol{G}_f = 25.9\ \mathrm{s}/(s^2 + 23.17\ \mathrm{s} + 9.78)$ that captures the frequency content of ρ is used in the synthesis algorithm of Sec. V.C.2. Theorem IV.3 is satisfied with $\xi = 4.519$ and a bounded region of initial condition

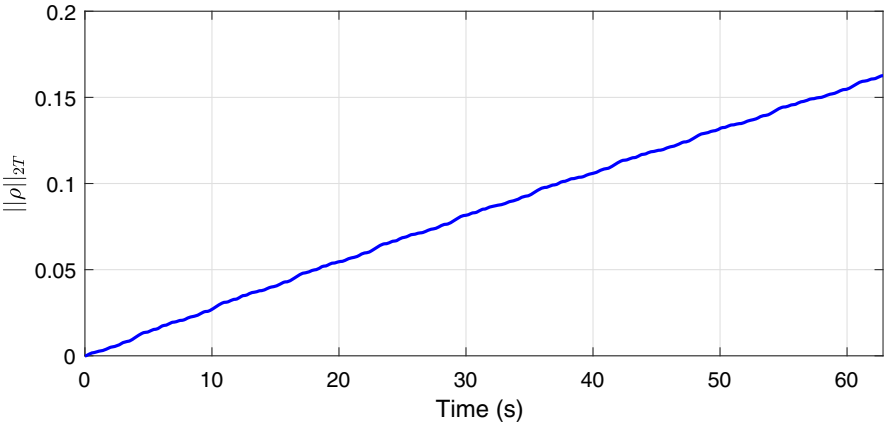

Fig. 3 The $\|\rho\|_{2T}$ transient bounding for general and filtered excitation signal of the fluid-inspired model in Sec. VI.

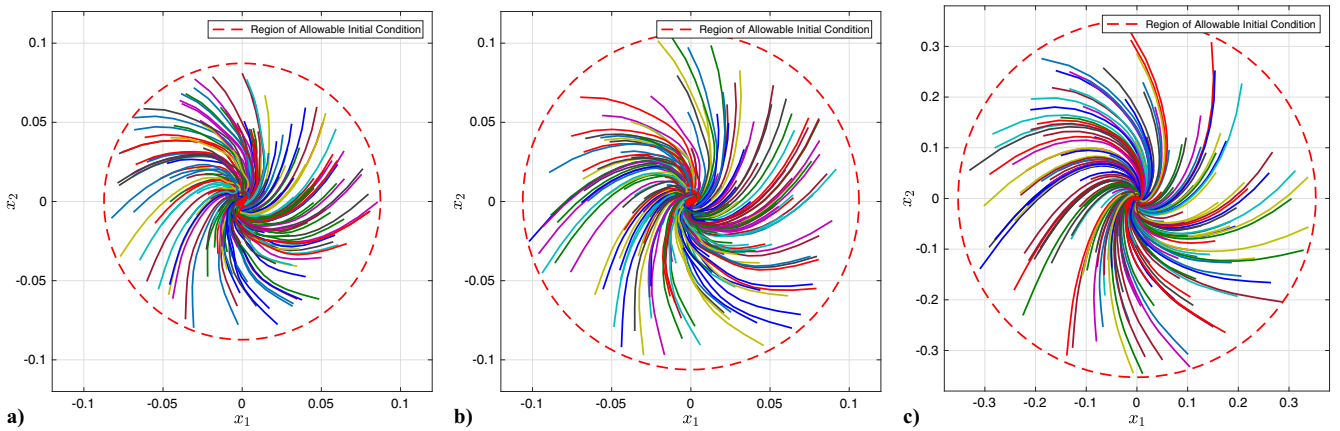

Fig. 4 Phase portrait response of the two-state fluid-inspired model of Sec. VI with external excitation of ρ and with controllers synthesized using algorithms based on a a) general excitation, b) filtered excitation, and c) harmonic excitation. The region of allowable initial condition is indicated by a dashed red circle. Note that the axes of (c) are scaled differently from those of (a) and (b) to ensure legibility.

Table 1 Results of fluid-inspired two-state nonlinear model (region of allowable initial condition)

Synthesis approach	ξ	Allowable $\|x(0)\|_2$
No exogenous signal	— —	0.48
No exogenous signal with transient bounds	1.2467	0.385
Harmonic excitation	1.2435	0.3529
Filtered excitation	4.519	0.1062 (for $\|\rho\|_{2T} = 0$)
General excitation	5.4953	0.0873 (for $\|\rho\|_{2T} = 0$)

of $\|\boldsymbol{x}(0)\|_2 \leq 0.1062$ when $\|\rho\|_{2T} = 0$. Similar to the previous case of general excitation, as $\|\rho\|_{2T}$ grows with time, the region of allowable initial conditions shrinks to satisfy Eq. (62).

Finally, by augmenting the linear states with harmonic states, the algorithm in Sec. V.D.2 that satisfies Theorem IV.4 yields $\xi = 1.2435$ with a constant $\bar{\boldsymbol{\beta}}_0 = 0.1565$, which results in the $\|\boldsymbol{x}(0)\|_2 \leq 0.3529$ region of the allowable initial condition. Unlike the previous two approaches of general excitation and filtered excitation, using augmented harmonic states does not have a time-dependent region of allowable initial condition since the introduced exogenous signal is captured within the linear states and has been defined to be very gradually decreasing.

The increasingly enlarged region of allowable initial conditions is made possible by increasing the constraints of the exogenous signal given additional knowledge. Figure 4 shows the phase portrait response of the fluid-inspired closed-loop system with the three different synthesized controller. Each of the 200 trajectories is initiated within the region of allowable initial conditions. The results are listed in Table 1.

VII. Numerical Example with a Hypersonic Vehicle

The numerical example in Sec. VI for the fluid-inspired model demonstrated the effectiveness of modeling the exogenous signal as harmonic states compared to the other synthesis methods. This method is applied to a nonlinear hypersonic vehicle model in this section.

A. Hypersonic Model Dynamics

This section presents a slightly modified version of the control-oriented hypersonic model from [25] and reformulates the dynamics to a form that is amenable to the proposed control synthesis approach. The harmonic excitation signals used as part of a flight test are also described and formulated in a manner that they can be incorporated within the hypersonic model and accounted for within the control synthesis procedure.

The hypersonic vehicle model considered in this paper is based on a longitudinal control-oriented model described in [25] with the engine dynamics removed to reduce the number of states and remove an element of complexity in this investigation. It is worth noting that there is no fundamental limitation preventing the proposed control method from being applied to the full model in [25]. Although the additional complexities of the vehicle's engine dynamics are not included in this work, this will be examined in future work. The nonlinear equations of motion of the hypersonic vehicle are

$$\dot{V} = \frac{1}{m}[T(\alpha, \Phi)\cos\alpha - D(V, \alpha)] - g\sin(\theta - \alpha) \tag{87}$$

$$\dot{\alpha} = \frac{1}{mV}[-T(\alpha, \Phi)\sin\alpha - L(\alpha)] + Q + \frac{g}{V}\cos(\theta - \alpha) \tag{88}$$

$$\dot{\theta} = Q \tag{89}$$

$$\dot{Q} = \frac{1}{I_{yy}} M(V, \alpha, \delta_e, \Phi) \tag{90}$$

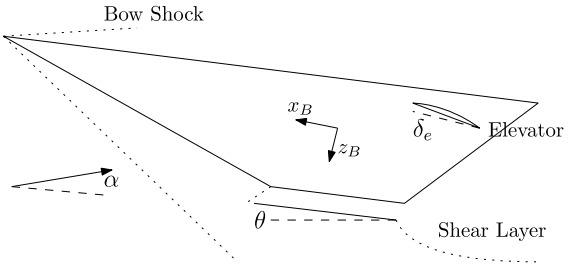

Fig. 5 Schematic of the longitudinal hypersonic model in [25].

where V is the vehicle's velocity, α is the vehicle's angle of attack, θ is the vehicle's pitch angle, and Q is the vehicle's pitch rate. The vehicle's mass is given by m, while its moment of inertia about the pitch axis is I_{yy}. The control inputs are specified as the elevator deflection δ_e and the fuel-to-air ratio Φ. The thrust, drag, lift, and moment acting on the vehicle are nonlinear functions of the state and input and are denoted as $T(\alpha, \Phi)$, $D(V, \alpha)$, $L(\alpha)$, and $M(V, \alpha, \delta_e, \Phi)$, respectively. Some of the states are illustrated in the simplified schematic of Fig. 5.

As described in [25], these nonlinear state- and input-dependent functions are obtained through compressible flow theory and are analytically intractable. Furthermore, direct application of nonlinear design methodologies, such as feedback linearization, to the truth model governing equations is not possible with implicit functions of the state and input variables. The control-oriented model is a curve fit and simplified model that was used for the application of an approximate feedback linearization technique.

The nonlinear dynamics described by Eqs. (87) through (90) can be written in terms of the nonlinear ordinary differential equation $\dot{\boldsymbol{x}} = \boldsymbol{f}(\boldsymbol{x}, \boldsymbol{u})$, where the state is defined as $\boldsymbol{x} = [V\ \alpha\ \theta\ Q]^{\mathsf{T}}$ and the inputs are given by $\boldsymbol{u} = [\delta_e\ \Phi]^{\mathsf{T}}$. The system's nonlinear dynamics can be linearized about a trim point. Only the elevator angle δ_e is set as an input to the dynamic system in this particular numerical example.

B. Numerical Results

Numerical simulations are performed with the nonlinear hypersonic vehicle longitudinal model described in Sec. VII.A. Numerical results in this section are presented for scenarios with and without external harmonic signals to the elevator angle δ_e. The trim condition with states $V_0 = 9962$ ft/s, $\alpha_0 = 2.3°$, $\theta_0 = 0.9768°$, and $Q_0 = 0$ deg/s and inputs $\delta_{e0} = 13°$ and $\Phi = 0.1294$ is chosen.

The nonlinearities of the control-oriented model are characterized by the following functions:

$$\boldsymbol{f}_1 = \frac{1}{m} T(\alpha, \Phi)\cos\alpha \mathbf{1}_1 \tag{91}$$

$$\boldsymbol{f}_2 = \frac{-1}{m} D(V, \alpha)\mathbf{1}_1 \tag{92}$$

$$\boldsymbol{f}_3 = -g\sin(\theta - \alpha)\mathbf{1}_1 \tag{93}$$

$$\boldsymbol{f}_4 = \dot{\alpha}\mathbf{1}_2 \tag{94}$$

$$\boldsymbol{f}_5 = \dot{Q}(V, \alpha, \delta_e, \Phi)\mathbf{1}_4 \tag{95}$$

such that $\boldsymbol{f} = \sum_i^{n_p} \boldsymbol{f}_i$, as described in Eq. (7). The sampling region of $\mathbb{X}_c \times \mathbb{U}_c$ is defined as $\mathbb{X}_c = \mathcal{E}(\boldsymbol{W})$, with $\boldsymbol{W} = \text{diag}(50, 0.05, 0.05, 0.05)$ and $\mathbb{U}_c = \mathcal{B}(r)$ with $r = 0.161$. In this numerical example, the sampling of $\Delta_i, i \in \mathcal{N}_{n_p}$ is computed from the analytic control-oriented model in Eq. (8), though the methodology allows for the incorporation of data from other sources, such as from a lookup table of CFD data. The weighting matrix $\boldsymbol{E}_i, i \in \mathcal{N}_{n_p}$ is chosen such that $\|\boldsymbol{v}_i\|_2 \leq 1, i \in \mathcal{N}_{n_p}$. The bounds computed for $\boldsymbol{\Delta}$ are $\gamma_1^2 = 1.43682$, $\gamma_2^2 = 15.2734$, $\gamma_3^2 = 2.81978 \cdot 10^{-5}$, $\gamma_4^2 = 3.06664 \cdot 10^{-9}$, and $\gamma_5^2 = 0.00361895$.

Without the addition of any harmonic excitation signals, the sequential SDP synthesis method described in [22] is additionally constrained with transient bound constraints on the closed-loop response using Lemma IV.1. When solved, it yields $\xi = 1.935$ with bounded initial conditions within the set $\mathbb{X}_\star \in \xi^{-1}\mathcal{E}(\boldsymbol{W}) = 0.5168\mathcal{E}(\boldsymbol{W})$. Intuitively, this is a Euclidean ball with the vertex at approximately half of the diagonal of $\boldsymbol{W}$. For example, one of the vertices is $\delta V = 25.84$ ft/s with other terms within $\delta\boldsymbol{x} = 0$.

The exogenous signal considered here is made of three harmonic excitation signals with frequencies $\omega = \{1, 2, 3\}$ rad/s and amplitudes of $\delta_e = 0.15°$ added to the elevator input of the closed-loop system. The phase between the harmonic excitations is chosen as $\boldsymbol{\phi} = \{-88.8085°, -177.6169°, -266.4254\}$ in the numerical results. The choice of frequencies and amplitudes is in a somewhat arbitrary fashion, though as reference, the linearized system's natural frequencies are 0.0047, 2.31, and 2.2174 rad/s. The phase is chosen such that the amplitude of the excitation signal is approximately 0 at $t = 0$ s. Artificial damping of $\mu = 0.003$ is applied to force a small exponential decay of the harmonic signal. The resulting signal is shown in Fig. 6 and represents the external harmonic excitation applied to the elevator angle input δ_e.

In Theorem IV.4, the bound on the region of allowable initial conditions $\mathcal{E}(\boldsymbol{W})$ depends not only on ξ but also on $\bar{\boldsymbol{\beta}}(0)^\mathsf{T}\bar{\boldsymbol{\beta}}(0)$, indicating that the initial conditions of the harmonic signal play a role in the bounding of the system states. By setting $\boldsymbol{\Pi} = 0.1 \cdot \max(\mathrm{diag}(\boldsymbol{\beta}))^{-1} = \mathrm{diag}(38.1972, 38.1972, 38.1972, 19.0986, 38.1972, 12.7324)$ for the change of coordinates, $\bar{\boldsymbol{\beta}}(0)^\mathsf{T}\bar{\boldsymbol{\beta}}(0) = 0.03$. This allows for tuning of the phase $\boldsymbol{\phi}$ to minimize ψ. The algorithm in Sec. V.D.2 is solved in MATLAB using `YALMIP` [32] and `MOSEK` [33], yielding a transient bound value of $\xi = 1.8824$ and the controller gain

$$\boldsymbol{K} = \begin{bmatrix} -0.0005 & 2.4608 & 0.5126 & 1.3894 \\ -0.0028 & 0.1242 & -0.9077 & -0.5698 \end{bmatrix} \tag{96}$$

Substituting this and $\|\boldsymbol{W}^{-1}\delta\boldsymbol{x}(T)\|_2 = 1$ into Eq. (67), the region of allowable initial conditions is found to be $\mathbb{X}_{\star h} = 0.5022\mathcal{E}(\boldsymbol{W})$.

Numerical simulations are performed on the longitudinal hypersonic vehicle with 200 different randomized initial conditions within the set $\mathbb{X}_{\star h}$, with the synthesized controller $\boldsymbol{K}$ and the harmonic excitation signal h applied to the elevator angle δ_e. All four states are shown in Fig. 7. The inputs from both the controller and the harmonic signal are shown in Fig. 8, where $\psi = 0.3723°$.

C. Discussion

In the scenario of no external harmonic excitations, the synthesized controller provides a guarantee of closed-loop asymptotic stability

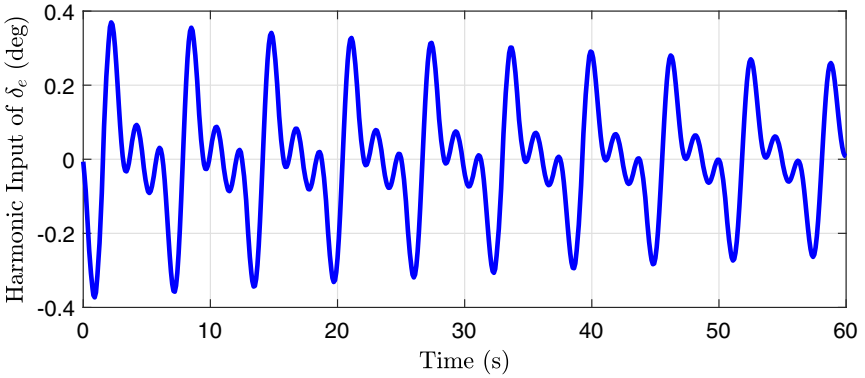

Fig. 6 The harmonic excitation signals applied to the closed-loop numerical simulations performed in Sec. VII.B.

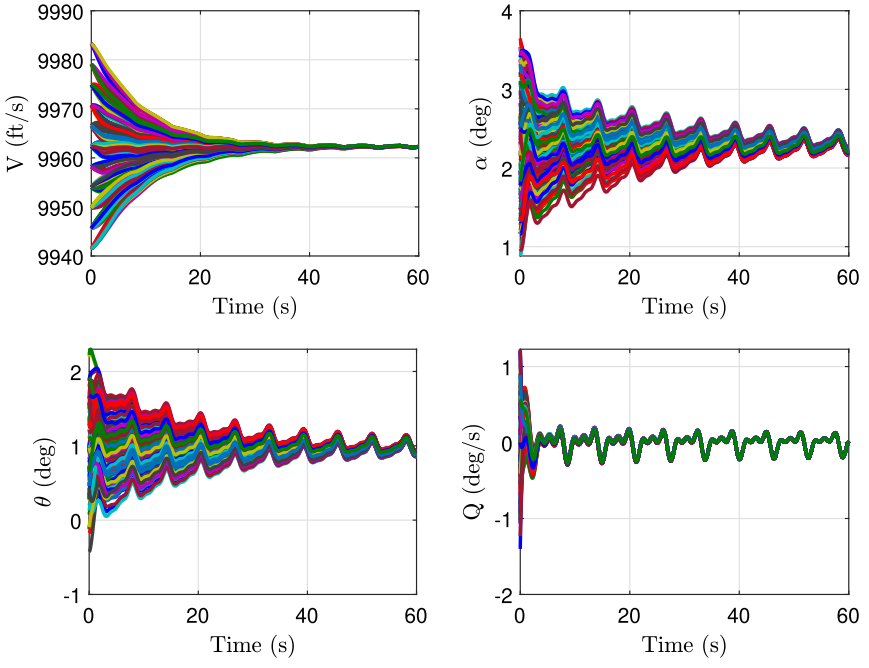

Fig. 7 Closed-loop results of the system states with 200 randomized sets of initial conditions from the numerical simulations performed in Sec. VII.B.

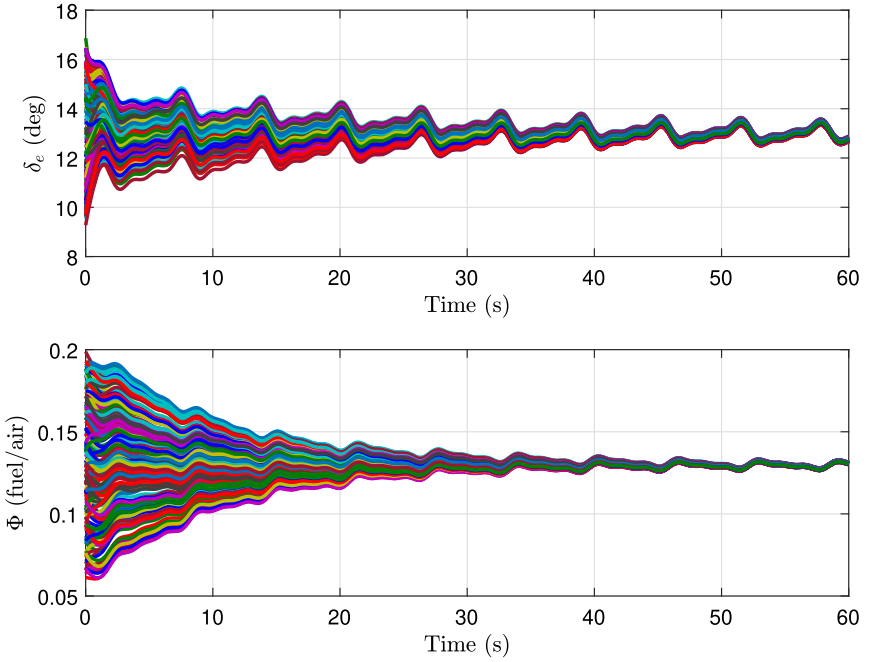

Fig. 8 Closed-loop results of the system inputs with 200 randomized sets of initial conditions from the numerical simulations performed in Sec. VII.B.

for the given region of attraction of $\mathbb{X}_\star = 0.5168\mathcal{E}(\boldsymbol{W})$, while still staying within bounds where the nonlinearities are adequately quantified through QCs. When an external harmonic excitation is present, asymptotic stability can no longer be guaranteed. Instead, a form of bounded output stability can be shown with the region of allowable initial conditions $\mathbb{X}_\star = 0.5022\mathcal{E}(\boldsymbol{W})$, which is confirmed through the numerical simulation results of Figs. 7 and 8. This is slightly smaller than the previous scenario due to the need to account for the energy that the excitation signal adds to the system.

When applied to a hypersonic vehicle prototype testing, our proposed method allows for the vehicle to take on any harmonic excitation maneuvers within the boundary of $\mathcal{E}(\boldsymbol{W})$; if for any reason this boundary is exceeded, the flight computer could switch to use the synthesized controller $\boldsymbol{K}$ to return to the flight trim condition. This could promote safe dynamic flight testing at the boundaries of the flight envelope while avoiding instability.

It is notable that the region of allowable initial conditions synthesized with the controller is conservative. Numerical simulations with initial conditions starting outside the region of allowable initial conditions are found to converge to a steady-state harmonic pattern within the sampling region $\mathbb{X}_c$. This is to be expected, as the control synthesis formulation is based on theorems with sufficient conditions for boundedness.

Scaling the variables was found to be especially important in this hypersonic example. This was achieved with the scaling matrix $\boldsymbol{E}$ and $\boldsymbol{W}$. In addition to normalizing the amplitudes, this approach accounts for the difference in units. The weighting matrix $\boldsymbol{W}$ can further be used as a design choice on emphasizing initial conditions in the different degrees of freedom.

VIII. Conclusions

This paper has presented a control synthesis method that ensures the boundedness of a nonlinear system's states in the presence of harmonic excitation inputs and with only input–output knowledge of the system's nonlinearities. This is an extension of the synthesis method presented in [22], which did not provide any transient bounds on the system's closed-loop response and did not account for any exogenous signals. The incorporation of transient bounds and harmonic excitation signals makes the proposed control synthesis amenable for hypersonic vehicle testing at conditions where the vehicle's nonlinearities are non-negligible, as shown through numerical simulation results.

Acknowledgments

This material is based upon work supported by the Office of the Under Secretary of Defense for Research and Engineering under award number FA9550-21-1-0213. S. K. Cheah's contributions were partially supported by a University of Minnesota Informatics Institute MnDRIVE Ph.D. Graduate Assistantship. M. S. Hemati acknowledges partial support from the Air Force Office of Scientific Research under award number FA9550-22-1-0004.

Appendix: Proof of Theorems IV.3 and IV.4

This appendix includes proofs of Theorems IV.3 and IV.4, which are similar to the proof of Theorem IV.2 but have subtle, yet important, distinctions.

A1. Proof of Theorem IV.3

Proof: The proof follows closely Theorem IV.2. The input is constrained similarly by Eqs. (64) and (42) to ensure that $\delta\boldsymbol{u} \in \mathbb{U}$. Defining the non-negative function $V = \boldsymbol{y}^\mathsf{T}\boldsymbol{P}\boldsymbol{y}$, where $\boldsymbol{P} > 0$, taking its time derivative, and using Eq. (21) yields

$$\dot{V} = \begin{bmatrix} \boldsymbol{y} \\ \boldsymbol{p} \\ \rho \end{bmatrix}^\mathsf{T} \begin{bmatrix} \boldsymbol{P}\boldsymbol{A}_b + \boldsymbol{A}_b^\mathsf{T}\boldsymbol{P} + \boldsymbol{P}\boldsymbol{A}_k + \boldsymbol{A}_k^\mathsf{T}\boldsymbol{P} & \boldsymbol{P}\hat{\boldsymbol{B}}_2 & \boldsymbol{P}\hat{\boldsymbol{B}}_f \\ * & \boldsymbol{0} & \boldsymbol{0} \\ * & * & -\zeta \end{bmatrix} \begin{bmatrix} \boldsymbol{y} \\ \boldsymbol{p} \\ \rho \end{bmatrix} + \zeta\rho^2 \tag{A1}$$

The inputs and outputs of each Δ_i can be rewritten as

$$\begin{bmatrix} \boldsymbol{v} \\ p_i \end{bmatrix} = \begin{bmatrix} \boldsymbol{E}_i[\boldsymbol{C}_i + \boldsymbol{D}_i\boldsymbol{K} & \boldsymbol{D}_i\boldsymbol{C}_f] & \boldsymbol{0} & \boldsymbol{0} \\ \boldsymbol{0} & & \boldsymbol{1}_i^\mathsf{T} & \boldsymbol{0} \end{bmatrix} \begin{bmatrix} \boldsymbol{y} \\ \boldsymbol{p} \\ \rho \end{bmatrix} \tag{A2}$$

With knowledge that $p_i^2 \le \gamma_i^2 \|\boldsymbol{v}_i\|_2$ is true pointwise in time for each $\Delta_i, \in \mathcal{N}_{n_p}$, this inequality can be written as

$$\begin{bmatrix} \boldsymbol{v}_i \\ p_i \end{bmatrix}^\mathsf{T} \begin{bmatrix} \gamma_i^2\boldsymbol{1} & \boldsymbol{0} \\ \boldsymbol{0} & -1 \end{bmatrix} \begin{bmatrix} \boldsymbol{v}_i \\ p_i \end{bmatrix} \ge 0 \tag{A3}$$

Returning to the norm bound of $\Delta_i, i \in \mathcal{N}_{n_p}$, multiplying both sides of Eq. (A3) by Eq. (A2) yields

$$\begin{bmatrix} \boldsymbol{y} \\ \boldsymbol{p} \\ \rho \end{bmatrix}^{\mathsf{T}} \begin{bmatrix} \gamma_i^2 \boldsymbol{\Phi}_i \boldsymbol{\Phi}_i^{\mathsf{T}} & \boldsymbol{0} & \boldsymbol{0} \\ \boldsymbol{0} & -\boldsymbol{1}_i \boldsymbol{1}_i^{\mathsf{T}} & \boldsymbol{0} \\ \boldsymbol{0} & \boldsymbol{0} & \boldsymbol{0} \end{bmatrix} \begin{bmatrix} \boldsymbol{y} \\ \boldsymbol{p} \\ \rho \end{bmatrix} \geq 0 \tag{A4}$$

Applying the Schur complement to Eq. (63) results in

$$\begin{bmatrix} \boldsymbol{P}\boldsymbol{A}_b + \boldsymbol{A}_b^{\mathsf{T}}\boldsymbol{P} + \boldsymbol{P}\boldsymbol{A}_k + \boldsymbol{A}_k^{\mathsf{T}}\boldsymbol{P} & \boldsymbol{P}\hat{\boldsymbol{B}}_2 & \boldsymbol{P}\hat{\boldsymbol{B}}_f \\ * & \boldsymbol{\Lambda} & \boldsymbol{0} \\ * & * & -\zeta \end{bmatrix} - \begin{bmatrix} \boldsymbol{\Theta} \\ \boldsymbol{0} \\ \boldsymbol{0} \end{bmatrix} \boldsymbol{\Xi}^{-1} \begin{bmatrix} \boldsymbol{\Theta} \\ \boldsymbol{0} \\ \boldsymbol{0} \end{bmatrix}^{\mathsf{T}} < 0 \tag{A5}$$

Multiplying the left and right sides by $[\boldsymbol{y}^{\mathsf{T}} \quad \boldsymbol{p}^{\mathsf{T}} \quad \rho]$ and $[\boldsymbol{y}^{\mathsf{T}} \quad \boldsymbol{p}^{\mathsf{T}} \quad \rho]^{\mathsf{T}}$ and then substituting in Eq. (A1) results in

$$\dot{V} - \xi\rho^2 + \textstyle\sum_{i=1}^{n_p} \lambda_i \begin{bmatrix} \boldsymbol{y} \\ \boldsymbol{p} \\ \rho \end{bmatrix}^{\mathsf{T}} \begin{bmatrix} \gamma_i^2 \boldsymbol{\Phi}_i \boldsymbol{\Phi}_i^{\mathsf{T}} & \boldsymbol{0} & \boldsymbol{0} \\ \boldsymbol{0} & -\boldsymbol{1}_i \boldsymbol{1}_i^{\mathsf{T}} & \boldsymbol{0} \\ \boldsymbol{0} & \boldsymbol{0} & \boldsymbol{0} \end{bmatrix} \begin{bmatrix} \boldsymbol{y} \\ \boldsymbol{p} \\ \rho \end{bmatrix} < 0 \tag{A6}$$

Knowing that $\lambda_i > 0$, $i \in \mathcal{N}_{n_p}$, and Eq. (A4) is satisfied, the S-procedure [28, Chap. 2] implies $\dot{V} < \xi\rho^2$. Integrating $\dot{V} < -\xi\rho^2$ from $t = 0$ to $t = T$, where $T \in \mathbb{R}_{>0}$, yields $V(T) < V(0) + \xi \int_0^T \rho^2 \, \mathrm{d}t$. Applying the nonstrict Schur complement, Eq. (65) can be rewritten as $\xi^{-1} \bar{\boldsymbol{W}}^{-\mathsf{T}} \boldsymbol{C}_s^{\mathsf{T}} \boldsymbol{C}_s \bar{\boldsymbol{W}}^{-1} \leq \boldsymbol{P}$. The constraint (66) can be rewritten as $\boldsymbol{P} \leq \xi \boldsymbol{W}^{-\mathsf{T}} \boldsymbol{W}^{-1}$. Combining these results yields

$$\begin{aligned} \xi^{-1} \boldsymbol{y}(T)^{\mathsf{T}} \bar{\boldsymbol{W}}^{-\mathsf{T}} \boldsymbol{C}_s^{\mathsf{T}} \boldsymbol{C}_s \bar{\boldsymbol{W}}^{-1} \boldsymbol{y}(T) &\leq \boldsymbol{y}(T)^{\mathsf{T}} \boldsymbol{P} \boldsymbol{y}(T) \leq \boldsymbol{y}(0)^{\mathsf{T}} \boldsymbol{P} \boldsymbol{y}(0) \\ &+ \xi \int_0^T \rho^2 \, \mathrm{d}t \leq \xi \boldsymbol{y}(0)^{\mathsf{T}} \bar{\boldsymbol{W}}^{-\mathsf{T}} \bar{\boldsymbol{W}}^{-1} \boldsymbol{y}(0) + \xi \int_0^T \rho^2 \, \mathrm{d}t \end{aligned} \tag{A7}$$

Substituting $\bar{\boldsymbol{W}} = \mathrm{diag}(\boldsymbol{W}, \boldsymbol{1})$ and $\boldsymbol{C}_s \bar{\boldsymbol{W}}^{-1} = [\boldsymbol{W}^{-1} \quad \boldsymbol{0}]$ into Eq. (A7) yields

$$\begin{aligned} \xi^{-1} \boldsymbol{x}(T)^{\mathsf{T}} \boldsymbol{W}^{-\mathsf{T}} \boldsymbol{W}^{-1} \boldsymbol{x}(T) &\leq \xi (\boldsymbol{x}(0)^{\mathsf{T}} \boldsymbol{W}^{-\mathsf{T}} \boldsymbol{W}^{-1} \boldsymbol{x}(0) \\ &+ \boldsymbol{x}_f(0)^{\mathsf{T}} \boldsymbol{x}_f(0)) + \xi \int_0^T \rho^2 \, \mathrm{d}t \end{aligned} \tag{A8}$$

The initial condition of the filter states $\boldsymbol{x}_f$ can be set to $\boldsymbol{0}$ and multiplying by ξ results in

$$\left\| \boldsymbol{W}^{-1} \delta \boldsymbol{x}(T) \right\|_2^2 \leq \xi^2 \left(\left\| \boldsymbol{W}^{-1} \delta \boldsymbol{x}(0) \right\|_2^2 + \left\| \rho \right\|_{2_T}^2 \right) \tag{A9}$$

which completes the proof. □

A2. Proof of Theorem IV.4

Proof: The proof follows closely Theorem IV.3. The input is constrained similarly by Eqs. (69) and (42). Defining the nonnegative function $V = \boldsymbol{z}^{\mathsf{T}} \boldsymbol{P} \boldsymbol{z}, \boldsymbol{P} > 0$, taking its time derivative, and using Eq. (38) yields

$$\dot{V} = \begin{bmatrix} \boldsymbol{z} \\ \boldsymbol{p} \end{bmatrix}^{\mathsf{T}} \begin{bmatrix} \boldsymbol{P}\boldsymbol{A}_s + \boldsymbol{A}_s^{\mathsf{T}}\boldsymbol{P} + \boldsymbol{P}\boldsymbol{A}_k + \boldsymbol{A}_k^{\mathsf{T}}\boldsymbol{P} & \boldsymbol{P}\hat{\boldsymbol{B}}_2 \\ * & \boldsymbol{0} \end{bmatrix} \begin{bmatrix} \boldsymbol{z} \\ \boldsymbol{p} \end{bmatrix} \tag{A10}$$

The inputs and outputs of each Δ_i can be rewritten as

$$\begin{aligned} \begin{bmatrix} \boldsymbol{v} \\ p_i \end{bmatrix} &= \begin{bmatrix} \boldsymbol{E}_i \left[(\boldsymbol{C}_{3,i} + \boldsymbol{D}_{3,i} \boldsymbol{K}) & \boldsymbol{D}_{3,i} \bar{\boldsymbol{T}} \right] & \boldsymbol{0} \\ \boldsymbol{0} & & \boldsymbol{1}_i^{\mathsf{T}} \end{bmatrix} \begin{bmatrix} \boldsymbol{z} \\ \boldsymbol{p} \end{bmatrix} \\ &= \begin{bmatrix} \boldsymbol{\Phi}_i^{\mathsf{T}} & \boldsymbol{0} \\ \boldsymbol{0} & \boldsymbol{1}_i^{\mathsf{T}} \end{bmatrix} \begin{bmatrix} \boldsymbol{z} \\ \boldsymbol{p} \end{bmatrix} \end{aligned} \tag{A11}$$

With knowledge that $p_i^2 \leq \gamma_i^2 \| \boldsymbol{v}_i \|_2$ is true pointwise in time for each $\Delta_i, \in \mathcal{N}_{n_p}$, this inequality can be written as

$$\begin{bmatrix} \boldsymbol{v}_i \\ p_i \end{bmatrix}^{\mathsf{T}} \begin{bmatrix} \gamma_i^2 \boldsymbol{1} & \boldsymbol{0} \\ \boldsymbol{0} & -1 \end{bmatrix} \begin{bmatrix} \boldsymbol{v}_i \\ p_i \end{bmatrix} \geq 0 \tag{A12}$$

Returning to the norm bound of $\Delta_i, i \in \mathcal{N}_{n_p}$, multiplying both sides of Eq. (A12) by Eq. (A11) yields

$$\begin{bmatrix} \boldsymbol{z} \\ \boldsymbol{p} \end{bmatrix}^{\mathsf{T}} \begin{bmatrix} \gamma_i^2 \boldsymbol{\Phi}_i \boldsymbol{\Phi}_i^{\mathsf{T}} & \boldsymbol{0} \\ \boldsymbol{0} & -\boldsymbol{1}_i \boldsymbol{1}_i^{\mathsf{T}} \end{bmatrix} \begin{bmatrix} \boldsymbol{z} \\ \boldsymbol{p} \end{bmatrix} \geq 0 \tag{A13}$$

Applying the Schur complement to Eq. (68) results in

$$\begin{bmatrix} \boldsymbol{P}\boldsymbol{A}_s + \boldsymbol{A}_s^{\mathsf{T}}\boldsymbol{P} + \boldsymbol{P}\boldsymbol{A}_k + \boldsymbol{A}_k^{\mathsf{T}}\boldsymbol{P} & \boldsymbol{P}\hat{\boldsymbol{B}}_2 \\ * & \boldsymbol{\Lambda} \end{bmatrix} - \begin{bmatrix} \boldsymbol{\Theta} \\ \boldsymbol{0} \end{bmatrix} \boldsymbol{\Xi}^{-1} \begin{bmatrix} \boldsymbol{\Theta} \\ \boldsymbol{0} \end{bmatrix}^{\mathsf{T}} < 0 \tag{A14}$$

Multiplying the left and right sides of Eq. (A14) by $[\boldsymbol{z}^{\mathsf{T}} \quad \boldsymbol{p}^{\mathsf{T}}]$ and $[\boldsymbol{z}^{\mathsf{T}} \quad \boldsymbol{p}^{\mathsf{T}}]^{\mathsf{T}}$ and then substituting in Eq. (A10) results in

$$\dot{V} + \textstyle\sum_{i=1}^{n_p} \lambda_i \begin{bmatrix} \boldsymbol{z} \\ \boldsymbol{p} \end{bmatrix}^{\mathsf{T}} \begin{bmatrix} \gamma_i^2 \boldsymbol{\Phi}_i \boldsymbol{\Phi}_i^{\mathsf{T}} & \boldsymbol{0} \\ \boldsymbol{0} & -\boldsymbol{1}_i \boldsymbol{1}_i^{\mathsf{T}} \end{bmatrix} \begin{bmatrix} \boldsymbol{z} \\ \boldsymbol{p} \end{bmatrix} < 0 \tag{A15}$$

Knowing that $\lambda_i > 0$, $i \in \mathcal{N}_{n_p}$, and the inequality in Eq. (A13) is satisfied, the S-procedure [28, Chap. 2] implies that $\dot{V} < 0$.

Integrating $\dot{V} < 0$ from $t = 0$ to $t = T$, where $T \in \mathbb{R}_{>0}$, yields $V(T) \leq V(0)$ or $\boldsymbol{z}(T)^{\mathsf{T}} \boldsymbol{P} \boldsymbol{z}(T) \leq \boldsymbol{z}(0)^{\mathsf{T}} \boldsymbol{P} \boldsymbol{z}(0)$. Applying the nonstrict Schur complement, Eq. (70) can be rewritten as $\xi^{-1} \bar{\boldsymbol{W}}^{-\mathsf{T}} \boldsymbol{C}_s^{\mathsf{T}} \boldsymbol{C}_s \bar{\boldsymbol{W}}^{-1} \leq \boldsymbol{P}$. The constraint (71) can be rewritten as $\boldsymbol{P} \leq \xi \bar{\boldsymbol{W}}^{-\mathsf{T}} \bar{\boldsymbol{W}}^{-1}$. Combining these results yields

$$\begin{aligned} \xi^{-1} \boldsymbol{z}(T)^{\mathsf{T}} \bar{\boldsymbol{W}}^{-\mathsf{T}} \boldsymbol{C}_s^{\mathsf{T}} \boldsymbol{C}_s \bar{\boldsymbol{W}}^{-1} \boldsymbol{z}(T) &\leq \boldsymbol{z}(T)^{\mathsf{T}} \boldsymbol{P} \boldsymbol{z}(T) \\ &\leq \boldsymbol{z}(0)^{\mathsf{T}} \boldsymbol{P} \boldsymbol{z}(0) \leq \xi \boldsymbol{z}(0)^{\mathsf{T}} \bar{\boldsymbol{W}}^{-\mathsf{T}} \bar{\boldsymbol{W}}^{-1} \boldsymbol{z}(0) \end{aligned} \tag{A16}$$

Substituting $\bar{\boldsymbol{W}} = \mathrm{diag}(\boldsymbol{W}, \boldsymbol{1})$ and $\boldsymbol{C}_s \bar{\boldsymbol{W}}^{-1} = [\boldsymbol{W}^{-1} \quad \boldsymbol{0}]$ into Eq. (A16) and then multiplying by ξ results in

$$\delta \boldsymbol{x}(T)^{\mathsf{T}} \boldsymbol{W}^{-\mathsf{T}} \boldsymbol{W}^{-1} \delta \boldsymbol{x}(T) \leq \xi^2 \left(\delta \boldsymbol{x}(0)^{\mathsf{T}} \boldsymbol{W}^{-\mathsf{T}} \boldsymbol{W}^{-1} \delta \boldsymbol{x}(0) + \bar{\boldsymbol{\beta}}(0)^{\mathsf{T}} \bar{\boldsymbol{\beta}}(0) \right) \tag{A17}$$

which completes the proof. □

References

[1] Cheah, S. K., Bhattacharjee, D., Hemati, M., and Caverly, R., "Control Synthesis for a Hypersonic Vehicle with Harmonic Excitation Inputs and Input-Output-Sampled Nonlinearities," *AIAA SciTech 2024 Forum*, AIAA Paper 2024-1589, 2024. https://doi.org/10.2514/6.2024-1589

[2] Chavez, F. R., and Schmidt, D. K., "Analytical Aeropropulsive-Aeroelastic Hypersonic-Vehicle Model with Dynamic Analysis," *Journal of Guidance, Control, and Dynamics*, Vol. 17, No. 6, 1994, pp. 1308–1319. https://doi.org/10.2514/3.21349

[3] Williams, T., Bolender, M., Doman, D., and Morataya, O., "An Aerothermal Flexible Mode Analysis of a Hypersonic Vehicle," *AIAA Atmospheric Flight Mechanics Conference and Exhibit*, AIAA Paper 2006-6647, 2006. https://doi.org/10.2514/6.2006-6647

[4] Oppenheimer, M., Skujins, T., Bolender, M., and Doman, D., "A Flexible Hypersonic Vehicle Model Developed with Piston Theory," *AIAA Atmospheric Flight Mechanics Conference and Exhibit*, AIAA Paper 2007-6396, 2007.
https://doi.org/10.2514/6.2007-6396

[5] Bolender, M., and Doman, D., "A Non-Linear Model for the Longitudinal Dynamics of a Hypersonic Air-Breathing Vehicle," *AIAA Guidance, Navigation, and Control Conference and Exhibit*, AIAA Paper 2005-6255, 2005.
https://doi.org/10.2514/6.2005-6255

[6] Wang, Q., and Stengel, R. F., "Robust Nonlinear Control of a Hypersonic Aircraft," *Journal of Guidance, Control, and Dynamics*, Vol. 23, No. 4, 2000, pp. 577–585.
https://doi.org/10.2514/2.4580

[7] Zhao, D., Jiang, B., and Yang, H., "Backstepping-Based Decentralized Fault-Tolerant Control of Hypersonic Cehicles in PDE-ODE Form," *IEEE Transactions on Automatic Control*, Vol. 67, No. 3, 2021, pp. 1210–1225.
https://doi.org/10.1109/TAC.2021.3059689

[8] Xu, H., Mirmirani, M. D., and Ioannou, P. A., "Adaptive Sliding Mode Control Design for a Hypersonic Flight Vehicle," *Journal of Guidance, Control, and Dynamics*, Vol. 27, No. 5, 2004, pp. 829–838.
https://doi.org/10.2514/1.12596

[9] Ding, Y., Wang, X., Bai, Y., and Cui, N., "An Improved Continuous Sliding Mode Controller for Flexible Air-Breathing Hypersonic Vehicle," *International Journal of Robust and Nonlinear Control*, Vol. 30, No. 14, 2020, pp. 5751–5772.
https://doi.org/10.1002/rnc.5114

[10] Gibson, T., and Annaswamy, A., "Adaptive Control of Hypersonic Vehicles in the Presence of Thrust and Actuator Uncertainties," *AIAA Guidance, Navigation and Control Conference and Exhibit*, AIAA Paper 2008-6961, 2008.
https://doi.org/10.2514/6.2008-6961

[11] Groves, K., Sigthorsson, D., Serrani, A., Yurkovich, S., Bolender, M., and Doman, D., "Reference Command Tracking for a Linearized Model of an Air-Breathing Hypersonic Vehicle," *AIAA Guidance, Navigation, and Control Conference and Exhibit*, AIAA Paper 2005-6144, 2005.
https://doi.org/10.2514/6.2005-6144

[12] Keshmiri, S., Colgren, R., and Mirmirani, M., "Development of an Aerodynamic Database for a Generic Hypersonic Air Vehicle," *AIAA Guidance, Navigation, and Control Conference and Exhibit*, AIAA Paper 2005-6257, 2005.
https://doi.org/10.2514/6.2005-6257

[13] Gruhn, P., and Gülhan, A., "Aerodynamic Measurements of an Air-Breathing Hypersonic Vehicle at Mach 3.5 to 8," *AIAA Journal*, Vol. 56, No. 11, 2018, pp. 4282–4296.
https://doi.org/10.2514/1.J056522

[14] Dörfler, F., "Data-Driven Control: Part One of Two: A Special Issue Sampling from a Vast and Dynamic Landscape," *IEEE Control Systems Magazine*, Vol. 43, No. 5, 2023, pp. 24–27.
https://doi.org/10.1109/MCS.2023

[15] Dörfler, F., "Data-Driven Control: Part Two of Two: Hot Take: Why Not Go With Models," *IEEE Control Systems Magazine*, Vol. 43, No. 6, 2023, pp. 27–31.
https://doi.org/10.1109/MCS.2023.3310302

[16] De Persis, C., and Tesi, P., "Formulas for Data-Driven Control: Stabilization, Optimality, and Robustness," *IEEE Transationcs on Automatic Control*, Vol. 65, No. 3, 2020, pp. 909–924.
https://doi.org/10.1109/TAC.2019.2959924

[17] Hou, Z.-S., and Wang, Z., "From Model-Based Control to Data-Driven Control: Survey, Classification and Perspective," *Information Sciences*, Vol. 235, June 2013, pp. 3–35.
https://doi.org/10.1016/j.ins.2012.07.014

[18] Romer, A., Berberich, J., Köhler, J., and Allgöwer, F., "One-Shot Verification of Dissipativity Properties from Input-Output Data," *IEEE Control Systems Letters*, Vol. 3, No. 3, 2019, pp. 709–714.
https://doi.org/10.1109/LCSYS.2019.2917162

[19] Tanemura, M., and Azuma, S.-I., "Efficient Data-Driven Estimation of Passivity Properties," *IEEE Control Systems Letters*, Vol. 3, No. 2, 2018, pp. 398–403.
https://doi.org/10.1109/LCSYS.2018.2887241

[20] Bu, X., Wu, X., Huang, J., and Wei, D., "A Guaranteed Transient Performance-Based Adaptive Neural Control Scheme with Low-Complexity Computation for Flexible Air-Breathing Hypersonic Vehicles," *Nonlinear Dynamics*, Vol. 84, Feb. 2016, pp. 2175–2194.
https://doi.org/10.1007/s11071-016-2637-0

[21] Niu, J., Chen, F., and Tao, G., "Nonlinear Fuzzy Fault-Tolerant Control of Hypersonic Flight Vehicle with Parametric Uncertainty and Actuator Fault," *Nonlinear Dynamics*, Vol. 92, 2018, pp. 1299–1315.
https://doi.org/10.1007/s11071-018-4127-z

[22] Cheah, S. K., Bhattacharjee, D., Hemati, M. S., and Caverly, R. J., "Robust Local Stabilization of Nonlinear Systems with Controller-Dependent Norm Bounds: A Convex Approach with Input-Output Sampling," *IEEE Control Systems Letters*, Vol. 7, Dec. 2022, pp. 931–936.
https://doi.org/10.1109/LCSYS.2022.3229004

[23] Megretski, A., and Rantzer, A., "System Analysis via Integral Quadratic Constraints," *IEEE Transactions on Automatic Control*, Vol. 42, No. 6, 1997, pp. 819–830.
https://doi.org/10.1109/9.587335

[24] Morelli, E. A., "Flight-Test Experiment Design for Characterizing Stability and Control of Hypersonic Vehicles," *Journal of Guidance, Control, and Dynamics*, Vol. 32, No. 3, 2009, pp. 949–959.
https://doi.org/10.2514/1.37092

[25] Parker, J. T., Serrani, A., Yurkovich, S., Bolender, M. A., and Doman, D. B., "Control-Oriented Modeling of an Air-Breathing Hypersonic Vehicle," *Journal of Guidance, Control, and Dynamics*, Vol. 30, No. 3, 2007, pp. 856–869.
https://doi.org/10.2514/1.27830

[26] Zong, Q., Wang, F., Tian, B., and Su, R., "Robust Adaptive Approximate Backstepping Control of a Flexible Air-Breathing Hypersonic Vehicle with Input Constraint and Uncertainty," *Proceedings of the Institution of Mechanical Engineers, Part I: Journal of Systems and Control Engineering*, Vol. 228, No. 7, 2014, pp. 521–539.
https://doi.org/10.1177/0959651814525371

[27] Caverly, R. J., and Forbes, J. R., "LMI Properties and Applications in Systems, Stability, and Control Theory," *ArXiv*, 2019. http://arxiv.org/abs/1903.08599.

[28] Boyd, S., El Ghaoui, L., Feron, E., and Balakrishnan, V., *Linear Matrix Inequalities in System and Control Theory*, SIAM, Philadelphi, PA, 1994.

[29] Zhou, K., and Khargonekar, P. P., "Robust Stabilization of Linear Systems with Norm-Bounded Time-Varying Uncertainty," *Systems & Control Letters*, Vol. 10, No. 1, 1988, pp. 17–20.
https://doi.org/10.1016/0167-6911(88)90034-5

[30] Warner, E., and Scruggs, J., "Iterative Convex Overbounding Algorithms for BMI Optimization Problems," *IFAC PapersOnLine*, Vol. 50, No. 1, 2017, pp. 10,449–10,455.
https://doi.org/10.1016/j.ifacol.2017.08.1974

[31] Mushtaq, T., Seiler, P., and Hemati, M. S., "On the Convexity of Static Output Feedback Control Synthesis for Systems with Lossless Nonlinearities," *Automatica*, Vol. 159, Jan. 2024, Paper 111380.
https://doi.org/10.1016/j.automatica.2023.111380

[32] Lofberg, J., "YALMIP: A Toolbox for Modeling and Optimization in MATLAB," *IEEE International Conference on Robotics and Automation*, Inst. of Electrical and Electronics Engineers, New York, 2004, pp. 284–289.
https://doi.org/10.1109/CACSD.2004.1393890

[33] The MOSEK Optimization Toolbox for MATLAB Manual, Ver. 9.0, MOSEK ApS, 2019, http://docs.mosek.com/9.0/toolbox/index.html.

M. Oppenheimer
Associate Editor